HHS Public Access

Author manuscript

Immunity. Author manuscript; available in PMC 2023 April 12.

Published in final edited form as:

Immunity. 2022 April 12; 55(4): 623–638.e5. doi:10.1016/j.immuni.2022.03.009.

Epithelial STAT6 O-GlcNAcylation drives a concerted anti-helminth alarmin response dependent on tuft cell hyperplasia and Gasdermin C

Ming Zhao[1], **Kaiqun Ren**[1,2], **Xiwen Xiong**[3], **Yue Xin**[3], **Yujie Zou**[4], **Jason C. Maynard**[5], **Angela Kim**[1], **Alexander P. Battist**[1], **Navya Koneripalli**[1], **Yusu Wang**[4], **Qianyue Chen**[4], **Ruyue Xin**[4], **Chenyan Yang**[3], **Rong Huang**[3], **Jiahui Yu**[3], **Zan Huang**[1], **Zengdi Zhang**[1], **Haiguang Wang**[1], **Daoyuan Wang**[2], **Yihui Xiao**[2], **Oscar C. Salgado**[6], **Nicholas N. Jarjour**[6], **Kristin A Hogquist**[6,7], **Xavier S. Revelo**[1,6], **Alma L. Burlingame**[5], **Xiang Gao**[4], **Jakob von Moltke**[8], **Zhaoyu Lin**[4,*], **Hai-Bin Ruan**[1,6,*,#]

[1]Department of Integrative Biology and Physiology, University of Minnesota Medical School, Minneapolis, Minnesota, USA

[2]College of Medicine, Hunan Normal University, Changsha, Hunan, China

[3]School of Forensic Medicine, Xinxiang Medical University, Xinxiang, Henan, China

[4]MOE Key Laboratory of Model Animals for Disease Study, State Key Laboratory of Pharmaceutical Biotechnology, Model Animal Research Center, National Resource Center for Mutant Mice of China, Nanjing Drum Tower Hospital, School of Medicine, Nanjing University, Nanjing, China

[5]Department of Pharmaceutical Chemistry, University of California, San Francisco, San Francisco, California, USA

[6]Center for Immunology, University of Minnesota Medical School, Minneapolis, Minnesota, USA

[7]Department of Laboratory Medicine and Pathology, University of Minnesota, Minneapolis, Minnesota, USA

[*]Correspondence: Zhaoyu Lin, PhD, 12 Xuefu Road, Jiangbei New Area District; Nanjing, Jiangsu 210061, China. Linzy@nju.edu.cn.
[*]Correspondence: Hai-Bin Ruan, PhD, 2261 6th St SE, Minneapolis, MN 55455, USA. hruan@umn.edu.
[#]Lead contact

Author Contributions

M.Z. designed, performed, and analyzed most experiments, particularly STAT6- and GSDMC-related work. K.R. initiated the project and analyzed IEC$^{\Delta Ogt}$ and Tuft$^{\Delta Ogt}$ mice. X.X., Y.X., C.Y., R.H., and J.Y. generated and analyzed IEC$^{CA\text{-}STAT6\text{-}Tg}$ and ISC$^{\Delta Ogt}$ mice. Y.Z., Y.W., Q.C., R.X., X.G., and Z.L. generated *Gsdmc-floxed* mice and performed Gsdmc RNA ISH and *Gsdmc*$^{-/-}$;*Il10*$^{-/-}$ colitis. J.C.M. and A.L.B. performed mass spectrometric identification of STAT6 O-GlcNAc sites. A.K., A.P.B., N.K., D.W., and Y.X. assisted genotyping, DSS colitis, and qPCR. Z.H. and Z.Z. constructed lentiviruses. H.W., O.C.S, K.A.H, and X.S.R. performed flow cytometry. N.N.J. performed *Il4ra*$^{-/-}$ infection. J.v.M. provided reagents and guidance to helminth infection and organoid culture. H.-B.R. conceived, designed, and performed experiments. M.Z. and H.-B.R. wrote the manuscript.

Inclusion and diversity

We worked to ensure sex balance in the selection of non-human subjects. One or more of the authors of this paper self-identifies as an underrepresented ethnic minority in science.

Conflict of Interest

The authors disclose no conflicts.

[8]Department of Immunology, University of Washington School of Medicine, Seattle, Washington, USA

Summary

The epithelium is an integral component of mucosal barrier and host immunity. Following helminth infection, the intestinal epithelial cells secrete “alarmin” cytokines, such as interleukin-25 (IL-25) and IL-33, to initiate the type 2 immune responses for helminth expulsion and tolerance. However, it is unknown how helminth infection and the resulting cytokine milieu drive epithelial remodeling and orchestrate alarmin secretion. Here we report that, epithelial O-linked N-Acetylglucosamine (O-GlcNAc) protein modification was induced upon helminth infections. By modifying and activating the transcription factor STAT6, O-GlcNAc transferase promoted the transcription of lineage-defining *Pou2f3* in tuft cell differentiation and IL-25 production. Meanwhile, STAT6 O-GlcNAcylation activated the expression of *Gsdmc* family genes. The membrane pore formed by GSDMC facilitated the unconventional secretion of IL-33. GSDMC-mediated IL-33 secretion was indispensable for effective antihelminth immunity and contributed to induced intestinal inflammation. Protein O-GlcNAcylation can be harnessed for future treatment of type 2 inflammation-associated human diseases.

Graphical Abstract

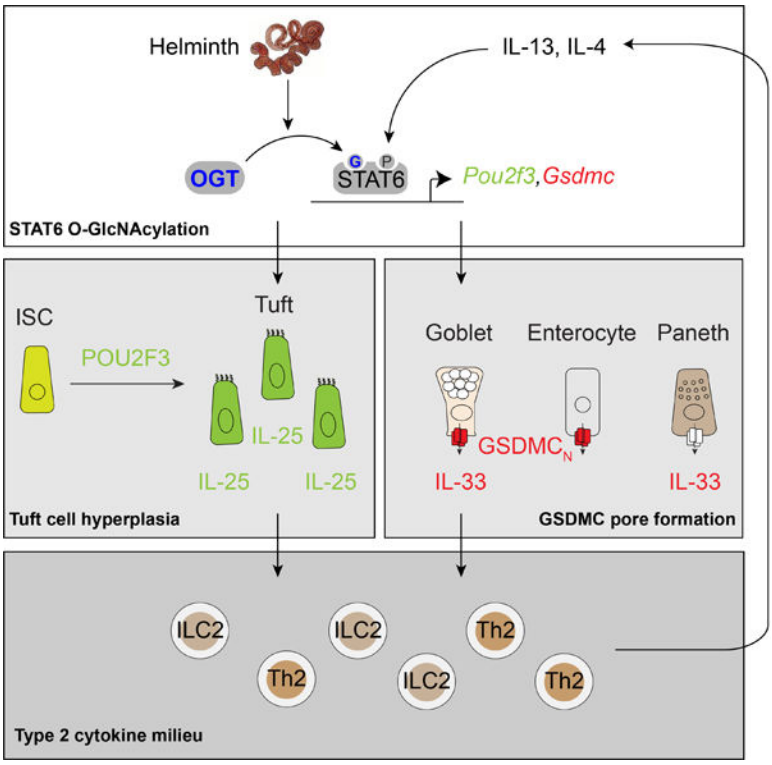

eTOC blurb

STAT6 is requisite for anti-helminth immunity, but it is presently unclear how STAT6 activity is finetuned to orchestrate “alarmin” cytokine responses. Zhao et al reveal that O-GlcNAc

modification allows STAT6 to drive the differentiation of IL-25-producing tuft cells and facilitate the unconventional IL-33 secretion via GSDMC membrane pores.

Keywords

O-GlcNAcylation; Gasdermin; Tuft cell; IL-33; colitis; IL-10

Introduction

More than 1.5 billion people are infected with helminths worldwide, predominantly distributed in tropical and subtropical areas. On the other hand, in developed countries with markedly reduced infectious diseases, there is a continuing increase in the incidences of inflammatory diseases. An under-stimulated immune system resulting from the absence of exposure to pathogens, in particular helminths, predisposes to autoimmune and allergic inflammation (Yazdanbakhsh et al., 2002; Molodecky et al., 2012; Bach, 2018). There is a growing interest in the use of helminth therapy for inflammatory bowel disease (IBD) and other autoimmune diseases (Smallwood et al., 2017); however, experimental and clinical data have been so far inconclusive. A greater understanding of host defense mechanisms against helminths is essential for the development of effective and safe treatments for intestinal infections and inflammation.

Type 2 immunity protects the host against tissue damage and helminth parasitism (Oliphant et al., 2011; Allen and Sutherland, 2014; Wynn, 2015). Type 2 cytokines, including interleukin-13 (IL-13), IL-5, IL-9, and IL-4, mobilize a broad range of downstream events, such as smooth muscle contraction, mucous secretion, and luminal fluidity, to promote the “weep and sweep” process for worm expulsion (Anthony et al., 2007). The intestinal epithelial cells (IECs) are the first responders to invading helminths. Activated IECs secrete “alarmins” like thymic stromal lymphopoietin (TSLP), IL-25, and IL-33 to inform and guide group 2 innate lymphoid cells (ILC2s) and CD4+ T helper 2 (Th2) cells for a coordinated type 2 reaction (Harris and Loke, 2017; Smallwood et al., 2017; Lloyd and Snelgrove, 2018).

Epithelial tuft cells, instructed by type 2 cytokines and microbiota-derived metabolites (Lei et al., 2018; Nadjsombati et al., 2018; Schneider et al., 2018), are the sole source of IL-25 (Gerbe et al., 2016; Howitt et al., 2016; von Moltke et al., 2016). A feed forward loop comprised of tuft cells, ILC2s, and epithelial progenitors supports the epithelial remodeling (Schneider et al., 2019; Ting and von Moltke, 2019). Chemosensory tuft cells not only initiate anti-parasite immune responses but also reduce chronic gut inflammation (Banerjee et al., 2020). Tuft cell development is specified by transcription factors including STAT6, POU2F3, and GFI1B (Bjerknes et al., 2012; Gerbe et al., 2016; Howitt et al., 2016; von Moltke et al., 2016; Schubart et al., 2019), but it is unclear how these transcription factors work in concert downstream of type 2 cytokines to direct tuft cell differentiation.

IL-33 is requisite for IL-13-driven type 2 responses (Hung et al., 2013). As a nuclear cytokine of the IL-1 family, IL-33 lacks signal sequences, thus does not follow the conventional route of secretion. Proinflammatory IL-1 family cytokines IL-1β and IL-18 are

cleaved by inflammasome-activated caspase-1 and released through pyroptotic membrane pores formed by the N-terminal domain of Gasdermin proteins (Broz et al., 2020). In contrast, proteolytic maturation of IL-33 largely happens extracellularly and is not required for its release and basal activity (Morita et al., 2017; Cayrol et al., 2018). IL-33 has been proposed to be both passively released from necrotic cells and actively released in the absence of cell death (Kouzaki et al., 2011; O'Grady et al., 2013; Uchida et al., 2017; Srisomboon et al., 2020). Nevertheless, mechanisms of active IL-33 secretion during homeostasis and inflammation remain mostly enigmatic (Zhao and Hu, 2010; Cayrol and Girard, 2018).

In this study, we investigated protein modification by a single O-linked N-Acetylglucosamine (O-GlcNAc) moiety at serine or threonine residues, termed O-GlcNAcylation in intestinal homeostasis and mucosal host defense. Analogous to phosphorylation, O-GlcNAcylation plays a central role in signaling pathways relevant to chronic human diseases such as diabetes, cancer, and immune disorders (Ruan et al., 2013b; Yang and Qian, 2017; Chang et al., 2020). O-GlcNAc transferase (OGT), using UDP-GlcNAc derived from the hexosamine biosynthetic pathway as the substrate (Figure S1A), controls diverse biological processes such as gene transcription, protein stability, and cell signaling (Hanover et al., 2012; Ruan et al., 2012; Ruan et al., 2013a; Ruan et al., 2014). O-GlcNAcase (OGA) mediates the removal of O-GlcNAcylation from proteins. We and others have demonstrated that protein O-GlcNAcylation senses glucose availability (Ruan et al., 2012; Hardiville and Hart, 2014), hormonal cues (Whelan et al., 2008; Ruan et al., 2014; Ruan et al., 2017), cellular stress (Martinez et al., 2017; Ruan et al., 2017), and immune and bacterial signals (Zhao et al., 2018; Liu et al., 2019; Chang et al., 2020; Zhao et al., 2020). Here, we show that STAT6 O-GlcNAcylation, by promoting the differentiation of IL-25-producing tuft cells and facilitating IL-33 secretion from IECs, functions as a posttranslational regulatory switch to turn on epithelial alarmin responses to helminths, thus initiating type 2 immune responses for tissue repair and inflammation control.

Results

Epithelial OGT is required for the tuft cell hyperplasia and helminth expulsion.

When infecting its natural host mouse (Camberis et al., 2003), the helminth *Heligmosomoides polygyrus* induced the expression of intestinal alarmin genes including *Il25*, *Il33* and *Tslp* (Figure S1B). Along with the rapid induction of a type 2 reaction as shown by STAT6 tyrosine phosphorylation, *H. polygyrus* infection increased and sustained global protein O-GlcNAcylation in the small intestine (Figure 1A and Figure S1C, D), indicative of the potential involvement of O-GlcNAcylation in regulating anti-helminthic STAT6 signaling. We generated *Vil1-Cre*;$Ogt^{F/Y}$ mice to delete the X-chromosome-located *Ogt* gene specifically in IECs ($IEC^{\Delta Ogt}$). Both tuft cell number (Figure 1B, C) and the expression of its marker genes including *Dclk1*, *Trpm5*, *Gfi1b, and Pou2f3* were reduced in naïve $IEC^{\Delta Ogt}$ mice (Figure 1D), when compared to wildtype littermates. The observed tuft cell defect was not caused by common protozoa colonization or difference thereof (Figure S1E, F). *H. polygyrus* infection led to tuft cell hyperplasia in wildtype mice as expected, but not in $IEC^{\Delta Ogt}$ mice (Figure 1E, F). As a result, the expression of tuft cell-restricted

Il25 was diminished in infected IEC$^{\Delta Ogt}$ mice (Figure 1G), causing increased *H. polygyrus* egg output into the feces (Figure 1H). This increased egg output in IEC$^{\Delta Ogt}$ mice was not because of reduced helminth colonization (Figure S1G).

The nematode *Nippostrongylus brasiliensis* induces a stronger type 2 immune response in mice that clears worms in 7–10 days. Similar to what were observed after *H. polygyrus* infection, *N. brasiliensis*-induced tuft cell hyperplasia (Figure 1I, J) and *Il25* expression (Figure 1K) were largely ablated in IEC$^{\Delta Ogt}$ mice. Impaired *N. brasiliensis* expulsion was observed in IEC$^{\Delta Ogt}$ mice, as shown by increased live worms in the intestine (Figure 1L) and more eggs produced in the feces (Figure 1M), when compared to wildtypes. These results show that intestinal epithelial O-GlcNAc signaling is indispensable for tuft cell development, IL-25 secretion, and anti-helminth responses.

Epithelial OGT deficiency impairs type 2 immunity.

Tuft cell-derived IL-25 initiates a type 2 immunity – IEC circuit for anti-helminth responses (Harris and Loke, 2017; Diefenbach et al., 2020). As a result of defective tuft cell hyperplasia, IEC$^{\Delta Ogt}$ mice at 14 days post *H. polygyrus* infection showed a reduced frequency of Th2 cells (Figure 2A, B and Figure S2A) and reduced proliferation of ILC2 cells in the lamina propria (Figure 2C, D). ILC2 number did not change after infection (Ferrer-Font et al., 2020) and was comparable between the two genotypes (Figure S2B, C). Type 2 cytokine genes *Il13* and *Il4* (Figure 2E) and recruitment of eosinophils (Figure 2F, G and Figure S2D) were diminished in infected IEC$^{\Delta Ogt}$ mice. Helminth infection-activated type 2 cytokine milieu induces goblet cell hyperplasia and mucus hypersecretion for host protection. However, the increase in goblet cell number and size after *H. polygyrus* infection was largely blunted in IEC$^{\Delta Ogt}$ mice (Figure 2H–J). Defective type 2 responses in IEC$^{\Delta Ogt}$mice were not unique to the *H. polygyrus* infection. Upon *N. brasiliensis* infection, IEC$^{\Delta Ogt}$ mice showed lower *Il13* mRNA expression in the intestine than wildtype mice (Figure 2K). Goblet cell hyperplasia and hypertrophy were also ablated in *N. brasiliensis* infected IEC$^{\Delta Ogt}$ mice (Figure 2L–N). Together, these data establish the critical role of epithelial OGT in mounting anti-helminth type 2 immune responses.

OGT promotes the differentiation of tuft cells from intestinal epithelial progenitors.

To extend findings in IEC$^{\Delta Ogt}$ mice, we also overexpressed OGT in IECs using the *Rosa26-LSL-rOGT* line that harbors an inducible rat OGT transgene in the mouse *Rosa26* locus (Yang et al., 2020; Zhao et al., 2020) (Figure 3A). rOGT overexpression increased DCLK1 protein expression and tuft cell number in the small intestine (Figure 3B, C). Tuft cell hyperplasia following *H. polygyrus* infection was amplified in IEC$^{rOGT\text{-}Tg}$ mice (Figure 3C), while fecal eggs were reduced (Figure 3D). Conversely, when mouse O-GlcNAcase (mOGA) was overexpressed in IECs to reduce protein O-GlcNAcylation (Figure 3E), the expression of tuft cell markers was substantially reduced, even in uninfected IEC$^{mOGA\text{-}Tg}$ mice (Figure 3F). This shows that O-GlcNAc is required and also sufficient to drive helminth infection-associated epithelial remodeling.

Next, we sought to examine whether OGT acts in mature tuft cells to support anti-helminth immunity. We ablated OGT in tuft cells using the *Dclk1-CreER* mice (Figure

3G) (Westphalen et al., 2014). We could observe weaker protein O-GlcNAcylation in wildtype tuft cells than neighboring enterocytes (Figure 3H, top panels). After feeding with tamoxifen-spiked food, specific O-GlcNAc depletion in DCLK1^{+} cells was achieved in Tuft$^{\Delta Ogt}$ mice (Figure 3H and Figure S3A, B). Nonetheless, tuft cell numbers both at the steady state and after *H. polygyrus* infection were comparable between control and Tuft$^{\Delta Ogt}$ mice (Figure 3I, J and Figure S3C, D). In turn, goblet cell hyperplasia (Figure S3E) and fecal egg output (Figure 3K) were not affected by OGT deficiency in tuft cells. Similarly, tuft cell hyperplasia following *N. brasiliensis* infection was not impaired either in Tuft$^{\Delta Ogt}$ mice (Figure 3L, M). These data indicate that OGT in mature tuft cells is dispensable for their function.

To determine if OGT in epithelial progenitors promotes the differentiation toward tuft cells, we generated inducible OGT deletion in intestinal stem cells (ISC$^{\Delta Ogt}$) mice using the *Olfm4-CreERT2* line (Figure 3N) (Schuijers et al., 2014). Treating small intestinal organoids with 4-hydroxytamoxifen (4-OHT) to knock down the *Ogt* gene (Figure 3O), diminished the ability of IL-13 to induce *Dclk1* gene expression (Figure 3P). It is therefore concluded that OGT acts in intestinal stem cells, not tuft cells, to remodel the epithelium upon helminth infections.

Pou2f3 transcription and tuft cell development is driven by STAT6 O-GlcNAcylation.

IL-13 and IL-4 exert their biological effects via STAT6 activation. Whole body *Stat6*$^{-/-}$ mice show severe defects in tuft cell development and type 2 responses upon helminth infections (Khan et al., 2001; Howitt et al., 2016). On the other hand, IEC-specific STAT6 activation promotes tuft cell differentiation and protects against helminths (Schubart et al., 2019). To address how epithelial STAT6 activity is fine-tuned, we first cultured wildtype and *Stat6*$^{-/-}$ organoids that only contained epithelial cells and found that epithelial STAT6 was required for stochastic and IL-13-stimulated differentiation of tuft cells and goblet cells (Figure S4A, B). Our previous transcriptomic analysis has predicted a possible role of STAT signaling in regulating OGT-dependent gene expression in IECs (Zhao et al., 2018). Indeed, we observed strong STAT6 staining in the nucleus of OGT-sufficient IECs following *H. polygyrus* infection (Figure 4A), indicative of STAT6 activation; while OGT-deficient IECs showed diffused STAT6 cellular localization (Figure 4A, B). This observation was further confirmed by immunofluorescent (Figure 4C) and immunoblotting (Figure 4D) of tyrosine-641 phosphorylated (pY641) STAT6, which is activated by IL-13 and IL-4 and required for its nuclear translation. Nuclear location of STAT6 was not perturbed in Tuft$^{\Delta Ogt}$ mice (Figure S3F), again pointing to OGT's dispensability in mature tuft cells. We then sought to determine how OGT regulates STAT6 signaling activity.

In fact, STAT6 protein itself could be O-GlcNAc modified (Figure 4E) (Gewinner et al., 2004; Qin et al., 2017). OGT overexpression substantially increased STAT6 O-GlcNAcylation, with a concomitant elevation of STAT6 pY641 phosphorylation (Figure 4E). On the other hand, OGT inhibition with ST045849 or OSMI-1 suppressed IL-4-induced STAT6 tyrosine phosphorylation (Figure 4F). Importantly, STAT6 was O-GlcNAcylated in IECs, dependent on OGT (Figure 4G). O-GlcNAcylation downregulation in organoids by an OGT inhibitor (Figure 4H) or OGA overexpression (Figure 4I), diminished IL-4-stimulated

pY641-STAT6. Using a luciferase reporter containing two tandem copies of STAT6 binding sites (Mikita et al., 1996), we found that OGT promoted the transcriptional activity of STAT6, but a catalytically-dead (CD) OGT did not (Figure 4J). The OGT inhibitor OSMI-1 diminished basal and IL-4-stimulated STAT6 transcriptional activation (Figure 4K).

To identify sites of STAT6 O-GlcNAcylation, we immunopurified STAT6 from HEK 293 cells co-expressed with OGT and subjected it to liquid chromatography with tandem mass spectrometry using electron transfer dissociation. Three clusters of eight O-GlcNAcylation sites were identified (Table S1), with the first cluster (S643/T644/T645) right after Y641 and two clusters (S746/T7575/S778 and S810/S825) in the transactivation domain (TAD) (Figure 4L). The two clusters within the TAD domain were the major O-GlcNAc sites, as mutating these sites to alanine (mtTAD) essentially ablated STAT6 O-GlcNAcylation (Figure 4M) and reduced its transcriptional activity (Figure 4N). O-GlcNAc-mutant STAT6 did not show defects in IL-4-stimulated Y641 phosphorylation (Figure S4C–E), indicating tyrosine phosphorylation-independent regulation of STAT6 activity by OGT. Instead, we found that O-GlcNAc mutants promoted the inhibitory serine phosphorylation of STAT6 (Figure 4O) (Wang et al., 2004; Maiti et al., 2005), thus leading to reduced binding to the transcriptional co-activator P300 (Figure 4P) (Gingras et al., 1999). To examine if STAT6 O-GlcNAcylation is functionally important for tuft cell development, we did lentiviral transduction of STAT6 into organoids followed by IL-4 treatment. Compared to the wildtype, STAT6-mtTAD showed diminished ability to induce the expression of tuft cell marker genes including *Dcl1k*, *Pou2f3*, *Gfi1b*, and *Ptgs1* (Figure 4Q).

We then asked how STAT6 O-GlcNAcylation controls tuft cell development. POU2F3 is a lineage-defining transcription factor for tuft cells, and its gene expression was downregulated in the $IEC^{\Delta Ogt}$ intestine (Figure 1D). Using $Stat6^{-/-}$ organoids, we found that IL-4-induced upregulation of *Pou2f3* was absolutely dependent on STAT6 (Figure 4R). OGT overexpression increased the *Pou2f3* promoter activity (Figure 4S), while OGT inhibition by OSMI-1 suppressed it (Figure 4T). Co-immunoprecipitation could not detect any physical interaction between ectopically expressed OGT and POU2F3 proteins (Figure S4E). However, O-GlcNAcylation was required for STAT6 to promote *Pou2f3* transcription, as STAT6-mtTAD showed blunted activity in *Pou2f3* luciferase assay (Figure 4U). Taken together, our results show that epithelial OGT, via STAT6 O-GlcNAcylation-dependent transcription of *Pou2f3*, drives tuft cell differentiation, IL-25 secretion, and subsequent mounting of anti-helminth immunity.

Identifying Gsdmc genes as targets of STAT6 O-GlcNAcylation.

OGT mediates pleiotropic activities in intestinal homeostasis and inflammation. We sought to test whether STAT6 O-GlcNAcylation in IECs controls any other tuft cell- and IL-25-independent events in antihelminth immunity. RNA-seq of IECs from $IEC^{\Delta Ogt}$ mice revealed that *Gsdmc2*, *3*, and *4* were among the most downregulated genes (Figure 5A). The encoding GSDMC proteins are the least studied members of the Gasdermin family that can be cleaved to release the N-terminal pore forming domain (Broz et al., 2020). *Gsdmc1–4* genes reside in a cluster on mouse Chromosome 15 and *Gsdmc1* expression is not detectable in the mouse intestine (data not shown). RT-PCR and Immunoblotting confirmed the nearly

total ablation of *Gsdmc2–4* genes (Figure S5A) and GSDMC protein (Figure 5B) in the $IEC^{\Delta Ogt}$ intestine. On the other hand, *Gsdmc2–4* genes were among the most upregulated genes after treating wildtype organoids with IL-4 (Figure 5C). The drastic changes in *Gsdmc2–4* gene expression upon OGT deficiency or IL-4 signaling activation prompted us to investigate their regulation by STAT6 and their role in antihelminth immunity.

Compared to other Gasdermin genes, *Gsdmc2–4* had highest expression in the IECs (Figure 5D and Figure S5B) and were the only ones induced by *H. polygyrus* infection (Figure 5E) or IL-4 (Figure S5C). RNA in situ hybridization revealed that the expression of *Gsdmc2–4* genes was restricted to IECs (Figure 5F). The induction of expression peaked around day 6 after infection and was most prominent in crypts adjacent to *H. polygyrus* granulomas (Figure 5F). Moreover, GSDMC protein cleavage could be readily induced by *H. polygyrus* infection (Figure 5G), following the induction of O-GlcNAcylation and pY-STAT6 (Figure 1A). In infected IL-4Rα-deficient mice, in which both IL-13 and IL-4 signaling is disrupted, GSDMC expression and subsequent cleavage were completely absent (Figure 5H). While it is still unclear which enzyme(s) are responsible for epithelial GSDMC cleavage, IL-4 treatment could enhance the amounts of $GSDMC_N$ in cultured organoids (Figure 5I).

We went on to examine whether OGT controls *Gsdmc* gene expression by O-GlcNAcylating STAT6. Treating wildtype organoids with IL-4 for 6 hours, a time point that had not induced tuft cell and goblet cell markers such as *Pou2f3*, *Dclk1*, and *Muc2* (Figure S5D–F), increased mRNA amounts of *Gsdmc2–4* (Figure 5J, K). However, such effect of IL-4 was totally ablated in $Stat6^{-/-}$ organoids (Figure 5J, K), even after 2 days of treatment (Figure S5G). On the other hand, transgenic expression of a constitutively active STAT6 in the intestinal epithelium in mice significantly increased *Gsdmc2–4* gene expression (Figure 5L). To directly assess transcriptional regulation, we constructed a luciferase reporter for the *Gsdmc2* gene. *Gsdmc2* promoter activity was elevated when OGT was overexpressed, while suppressed by OGA overexpression or an OGT inhibitor, OSMI-1 (Figure 5M, N). In addition, wildtype STAT6 but not STAT6-mtTAD activated *Gsdmc2* promoter (Figure 5O). We also did lentiviral transduction of O-GlcNAc-sufficient and -deficient STAT6 into intestinal organoids, and found reduced endogenous *Gsdmc4* expression in STAT6-mtTAD organoids (Figure 5P). Worth noting, *Gsdmc* transcription was not dependent on tuft cells, as expression of *Gsdmc2–4* genes was maintained in uninfected $Pou2f3^{-/-}$ mice (Figure S5H). These results demonstrate that, in parallel with *Pou2f3* induction, STAT6 O-GlcNAcylation boosts *Gsdmc* family gene expression during helminth infections.

To determine the functional impact of GSDMC, we generated *Gsdmc1–4*-floxed mice and mated them with *Vil1-Cre* to produce $IEC^{\Delta Gsdmc}$ mice (Figure 5Q). *H. polygyrus*-induced hyperplasia of both tuft cells and goblet cells was diminished in $IEC^{\Delta Gsdmc}$ mice (Figure 5R–T). As a result, more worm eggs were present in the feces of $IEC^{\Delta Gsdmc}$ mice, compared to controls (Figure 5U). Collectively, these data establish GSDMC as a helminth infection-induced, STAT6- and O-GlcNAc-dependent protein that mediates type 2 immunity.

GSDMC mediates unconventional IL-33 secretion.

Culturing GSDMC-sufficient and -deficient organoids, followed by IL-4 treatment for 2 days, did not change the expression of goblet and tuft cell markers (Figure 6A and Figure

S6A, B) nor the number of these cells (Figure S6C, D). The release of cytosolic lactate dehydrogenase (LDH) into culture medium was slightly reduced in IEC$^{\Delta Gsdmc}$ organoids (Figure S6E), suggesting that GSDMC$_N$ pore could mediate membrane permeability. LDH concentrations before and after IL-4 treatment were far lower than Triton-X-induced permeabilization (Figure S6E), indicating no substantial pyroptosis happened. RNA sequencing revealed that both control and IEC$^{\Delta Gsdmc}$ organoids reprogramed the transcriptomics upon IL-4 stimulation, while very few differentially expressed genes between GSDMC-sufficient and -deficient cells were found before or after IL-4 treatment (Figure 6B and Figure S6F, G). This suggests that cell autonomous GSDMC is dispensable for IL-4-stimulated epithelial remodeling ex vivo. Moreover, we treated animals with mouse IL-4 and anti-IL-4 antibody complexes that mimic STAT6 activation (von Moltke et al., 2016), and found equally increased tuft cell and goblet cell markers in wildtype and IEC$^{\Delta Gsdmc}$ mice (Figure S6H), indicating that GSDMC is not required for appropriate IL-4 actions in vivo.

We went on to identify the cell-non-autonomous mechanism for GSDMC. In addition to tuft cell-derived IL-25, IL-33 is another alarmin requisite for type 2 immune activation (Hung et al., 2013). However, the cellular source and secretion mechanism of this unconventional nuclear cytokine are largely unknown. We hypothesized that the GSDMC$_N$ pore, analogous to GSDMD$_N$ in mediating IL-1β secretion, functions as a conduit for the release of intestinal epithelial IL-33. While being abundant in the lamina propria, IL-33 is also expressed by the epithelium and stimulates type 2 immunity (Hung et al., 2020). IL-33 staining was absent in epithelial cells but still present in lamina propria cells in IEC$^{\Delta Il33}$ mice (Figure S7A), demonstrating the specificity of IL-33 antibody used. Epithelial IL-33 did not co-localize with DCLK1$^+$ tuft cells in naïve or infected mice (Figure S7B). Instead, IL-33 was localized to goblet cells in the villus (Figure 6C–E) and Paneth cells in the crypt (Figure 6C–E and Figure S7C, D), that are both labelled by AG2 and FCGBP. The localization of crypt IL-33 in Paneth cells was confirmed by co-staining with Lysozyme (Figure S7E). In helminth-infected small intestine, *Gsdmc2–4* RNA was generally restricted in transit amplifying cells (Figure 6F). But at the protein level, GSDMC expression was more abundant in the villus than the crypt (Figure 6G), representing the spatial discordances between mRNAs and proteins in the intestinal epithelium (Harnik et al., 2021). Membrane localization of GSDMC was apparent after helminth infection (Figure 6G), suggesting active pore formation.

To test if GSDMC$_N$ pores promotes IL-33 secretion in cells, we generated an inducible GSDMC$_N$ overexpression plasmid and co-transfected it with IL-33. Doxycycline induced GSDMC$_N$ expression and IL-33 secretion into the culture medium, along with reduced IL-33 inside the cell (Figure 6H). The release was not merely a result of cell death, as supplementing osmoprotectant glycine to prevent pyroptosis-associated membrane rupture did not prevent IL-33 release (Figure 6H and Figure S7F). To determine if GSDMC was required for epithelial IL-33 secretion, we isolated fresh IECs from wildtype and IEC$^{\Delta Gsdmc}$ mice and incubated them in serum-free medium. IL-33 protein could be readily detected in the medium of wildtype cells by Immunoblotting and ELISA, but not in that of GSDMC-deficient IECs (Figure 6I, J). Consistent with the villus expression of GSDMC, the GSDMC-dependent secretion of IL-33 and LDH was more evident in the villus than the crypt (Figure 6J, K). In IL-4Rα-deficient IECs, in which GSDMC was absent even after

helminth infection, IL-33 secretion was essentially ablated (Figure 6L). Collectively, these results imply that GSDMC pore formation in villus epithelial cells, goblet cells included, controls the unconventional secretion of IL-33.

To determine if reduced IL-33 secretion accounts for defective antihelminth responses, we treated *H. polygyrus*-infected IEC$^{\Delta Gsdmc}$ mice with recombinant IL-33 (Figure 6M). Tuft cell numbers in IEC$^{\Delta Gsdmc}$ mice could be rescued by IL-33, to a level comparable to treated wildtype mice (Figure 6N). The reduction in goblet cell number and size observed in untreated IEC$^{\Delta Gsdmc}$ mice was also absent after IL-33 administration (Figure 6O, P). In turn, IL-33 decreased fecal egg output in IEC$^{\Delta Gsdmc}$ mice (Figure 6Q). IL-33 did not further boost antihelminth responses in wildtype mice, indicating that endogenous IL-33 and other alarmins were sufficient to drive normal type 2 immunity.

Epithelial GSDMC promotes type 2 inflammation.

Gasdermin family proteins have been linked to human inflammatory diseases. GSDMB SNPs are reported to increase susceptibility to IBD and asthma (Chao et al., 2017; Das et al., 2017), independent of pyroptosis (Rana et al., 2022). GSDMB overexpression in mice induces airway remodeling and an asthma phenotype (Das et al., 2016). GSDMD in macrophages restrains colitis (Ma et al., 2020), while epithelial GSDMD promotes IL-1β release and experimental colitis in mice (Bulek et al., 2020).

Following the administration of dextran sulfate sodium (DSS) to induce acute colitis in mice, there was a transient increase in the expression and cleavage of GSDMC in the colon (Figure 7A). When subjecting IEC$^{\Delta Gsdmc}$ mice and whole-body *Gsdmc*$^{-/-}$ mice to acute DSS colitis, no changes in weight loss or colitis severity were observed (Figure 7B, C and data not shown). We wondered if this was due to the low expression of GSDMC, so we pre-infected the mice with *H. polygyrus* to induce GSDMC expression (9–14 days after infection) during the acute damage phage of DSS (Figure S8A). Compared to uninfected mice, helminth infection and presumably the persisting type 2 inflammation, exacerbated acute colitis (Figure S8B, C). However, we did not observe noticeable changes in weight loss, colon length or histopathology between wildtype and *Gsdmc*$^{-/-}$ mice (Figure S8D–F), despite there was a trending decrease of inflammatory gene expression in *Gsdmc*$^{-/-}$ mice (Figure S8G). These results indicate GSDMC is not essential for acute DSS damage.

Since type 2 cytokines are suggested to be involved in the pathogenesis of chronic intestinal inflammation (Bamias and Cominelli, 2015), we then infected mice with *H. polygyrus* after the administration of DSS to induce GSDMC expression during the reparative phase (Figure 7D). Again, *H. polygyrus* infection aggravated colitis-associated body weight loss (Figure 7E). But IEC$^{\Delta Gsdmc}$ mice recovered faster from DSS-induced weight loss than their littermate controls (Figure 7F). Histological assessment of inflammatory cell infiltration and epithelial architecture (Figure 7G, H) and quantification of gene expression (Figure 7I) revealed potent resolution of inflammation in IEC$^{\Delta Gsdmc}$ mice. The immunoregulatory IL-10 is essential for intestinal homeostasis and IL-10-deficient mice develop spontaneous colitis (Kuhn et al., 1993). Notably, there was increased GSDMC expression and cleavage in young *Il10*$^{-/-}$ mice (Figure 7J). To test if GSDMC contributes to the development of colitis in *Il10*$^{-/-}$ mice, we generated *Gsdmc*$^{-/-}$;*Il10*$^{-/-}$ mice and subjected them to induced colitis. We

found profound protection from weight loss and colon shortening in *Gsdmc*$^{-/-}$;*Il10*$^{-/-}$ mice, in comparison with *Il10*$^{-/-}$ mice (Figure 7K, L). Taken together, our data establish a pivotal role of GSDMC in promoting colonic inflammation.

Discussion

During helminth infections, intestinal epithelial cells (IECs) are among first responders from the host to rapidly secrete “alarmin” molecules including IL-25 and IL-33, which in turn drive the type 2 immune activation and subsequent epithelial remodeling. This feedforward circuit is dependent on epithelial STAT6; however, the upstream regulation and downstream mechanisms of IEC-intrinsic STAT6 are not fully understood. In this study, we show that the O-GlcNAc modification of STAT6 by OGT is promptly induced by helminth infections and supports a concerted alarmin response by promoting IL-25 production from hyperplastic tuft cells and GSDMC-mediated unconventional IL-33 secretion from IECs. Our results reveal an important role of epithelial OGT, STAT6 O-GlcNAcylation, and GSDMC for protective immunity against helminths and intestinal homeostasis.

Protein posttranslational modifications provide versatile tools used by pathogens for their infections (Ribet and Cossart, 2010) and play fundamental roles in host immune responses (Liu et al., 2016). Since its discovery in 1980s, intracellular O-GlcNAcylation has been shown to be activated following diverse immunological stimuli and control the development and function of innate and adaptive immune cells, including but not limited to macrophages, neutrophils, NK cells, T cells, and B cells (Chang et al., 2020). Bacterial and viral signals, via pattern recognition receptors and antigen presentation, are capable of control donor substrate availability, enzyme expression or activity to fine tune O-GlcNAcylation within immune cells (Chang et al., 2020). Here, we provide evidence that intestinal epithelial O-GlcNAcylation is also responsive to helminth infections and required for proper type 2 immune activation and worm expulsion. With data not shown, we found that IL-13 or IL-4 did not evidently change O-GlcNAcylation in cultured cells and organoids. Succinate produced by helminths and gut microbiota can be detected by the succinate receptor (SUCNR1) on tuft cells to trigger type 2 immune responses (Lei et al., 2018; Nadjsombati et al., 2018). We did not observe noticeable changes of intestinal protein O-GlcNAcylation in succinate-fed or *Sucnr1*$^{-/-}$ mice (data not shown). Helminth-dependent signals that activate epithelial O-GlcNAcylation merit further investigations in the future.

The necessity of STAT6 for helminth-associated epithelial remodeling is supported by findings in *Stat6*$^{-/-}$ mice (Khan et al., 2001; Howitt et al., 2016) and intestinal organoids in this study. The sufficiency of epithelial STAT6 in driving tuft and goblet cell hyperplasia is demonstrated by IEC-specific constitutive STAT6 overexpression in two mouse models generated by Schubart et al. (2019) and us. Therefore, STAT6 activity must be precisely controlled during homeostasis and infection. Upon IL-13 or IL-4 stimulation, STAT6 is tyrosine phosphorylated by JAK kinases, dimerized via the SH2 domain, and then translocated to the nucleus for DNA binding and gene transcription. Notably, majority of O-GlcNAc sites we have identified are located in the proximity of STAT6 transactivation domain. Mutating these O-GlcNAc sites increases serine phosphorylation, diminishes cofactor binding and transcriptional activity, but has no effect on tyrosine phosphorylation. It

suggests that O-GlcNAcylation is not a prerequisite for tyrosine phosphorylation-dependent STAT6 dimerization and OGT could at the same time modify upstream regulators such as JAK kinases to control STAT6 tyrosine phosphorylation. OGT and O-GlcNAcylation are predominantly found in the nucleus of IECs (Zhao et al., 2018). We postulate that nuclear STAT6 needs to be O-GlcNAc modified for its optimum transcriptional activation. It is worth noting that, in addition to driving epithelial remodeling upon helminth infections, O-GlcNAc signaling in IECs is active in naïve conditions, thus maintaining the steady-state intestinal homeostasis (Zhao et al., 2018).

While absolutely required for helminth-induced epithelial remodeling (Howitt et al., 2016), it is unknown how STAT6 signaling drive tuft cell hyperplasia (Billipp et al., 2021). Here we demonstrated that STAT6 promotes the transcription of the *Pou2f3* gene, a transcription factor specifically defining the tuft cell lineage (Gerbe et al., 2016). O-GlcNAcylation is vital for basal, IL-13- or IL-4-stimulated, and infection-induced *Pou2f3* gene expression and tuft cell differentiation from the stem and progenitor compartment. Once differentiated, tuft cells are not dependent on OGT anymore, as tuft and goblet cell pool and helminth expulsion ability were largely intact in $Tuft^{\Delta Ogt}$ mice. Mature tuft cells rely on chemosensory membrane receptors, such as G protein-coupled taste receptors, cation channel TRPM5, and SUCNR1, to detect the presence of helminth worms and in turn secrete effector molecules, IL-25 and Cysteinyl leukotrienes (McGinty et al., 2020; Billipp et al., 2021). This raises the possibility that IL-13-STAT6 signaling might also not be necessary for effector function of mature tuft cells, which certainly requires future studies.

Recent evidence points to the cellular context of IL-33 in dictating anti-helminth immunity. While intestinal epithelial IL-33 stimulates ILC2s and helminth clearance, IL-33 derived from dendritic cells enhances regulatory T (Treg) cell function and impairs host-protective responses (Hung et al., 2020). As an IL-1 family cytokine that does not possess a signal peptide, IL-33 is exported from dendritic cells via the pore-forming protein perforin-2 (Hung et al., 2020). In this study, we identified the cellular source and secretion mechanism of IEC-derived IL-33. Epithelial IL-33 expression could be detected in goblet and Paneth cells, but not tuft cells. Paneth cell hyperplasia has been observed in the small intestine of helminth-infected mice (Kamal et al., 2002) and is controlled by IL-13, IL-4 and STAT6 signaling (Stockinger et al., 2014; Schubart et al., 2019). The involvement of Paneth cells and their derived IL-33 in anti-helminth immunity; however, is yet experimentally determined. In terms of secretion, we found that the membrane pore formed by $GSDMC_N$ is sufficient to act as a conduit to facilitate IL-33 export from IECs. This is analogous to the unconventional secretion of IL-1β and IL-18 via $GSDMD_N$ pores formed on myeloid cells after inflammasome activation (Broz et al., 2020). Compared to other Gasdermin family genes, *Gsdmc2–4* genes are highly expressed by IECs in the intestine and the only ones induced by worm infection. We also found that *Gsdmc2–4* are among the most upregulated genes by IL-4, consistent with a recent publication (Xi et al., 2021). Additionally, our current study demonstrated that *Gsdmc2–4* transcription is dictated by STAT6 O-GlcNAcylation and the loss of GSDMC in IECs renders mice less effective to expel helminths. Xi et al. (2021) proposed a correlation between $GSDMC_N$ and pyropotic cell death. However, the fact that helminth infections induce $GSDMC_N$ accumulation and increase goblet cell number argues against the substantial existence of goblet cell pyroptosis.

Instead, we show that $GSDMC_N$ pores support IL-33 secretion independently of pyroptosis. GSDMC can be cleaved by caspase-8 to form $GSDMC_N$ pores in cancer cells (Hou et al., 2020; Zhang et al., 2021). It is important to determine in the future whether intestinal epithelial cells utilize the same mechanisms for GSDMC activation and whether IL-33 effector function (stimulation vs. suppression of anti-helminth immunity) is dependent on what plasma membrane conduit is used for secretion.

Certain helminth species have a protective role in different mouse models of IBD (Varyani et al., 2017); however, *H. polygyrus* exacerbates bacterial, chemical, and T cell-mediated colitis (Pastille et al., 2017; Su et al., 2018). Likewise, type 2 immune responses have both protective and inflammatory effects on the intestine (Bamias and Cominelli, 2015). Using the DSS colitis model followed by *H. polygyrus* infection or in $Il10^{-/-}$ mice, we found that GSDMC exacerbated intestinal inflammation. Whether such effect is dependent on IL-33 is still unknown. IL-33 reportedly has both pro- and anti-inflammatory roles in IBD pathogenesis (Hodzic et al., 2017; Williams et al., 2019), attributed to divergences in experimental models, cellular origins, and molecular targets. Future investigations are needed to test the possibility that $GSDMC_N$-exported IL-33 from IECs drives type 2 inflammation while perforin-2-delivered IL-33 from myeloid cells serves an immunosuppressive role by activating Treg cells (Hung et al., 2020).

In conclusion, our data define O-GlcNAcylation a regulatory mechanism of intestinal epithelial STAT6 activation following helminth infections. STAT6 O-GlcNAcylation accelerates the establishment of type 2 immunity by orchestrating an alarmin reaction in the intestinal epithelium – IL-25 production from POU2F3-defined tuft cells and IL-33 secretion via membrane pores formed by $GSDMC_N$. The immunoregulatory O-GlcNAc signaling can be harnessed for the future treatment of helminth infections and type 2 inflammation-associated diseases.

Limitations of the study

Our study has not determined how O-GlcNAc signaling is activated during helminth infections. Both helminth-derived molecules and tissue damage-associated signals warrant future investigations. While we only focused STAT6 O-GlcNAcylation, OGT could modify non-STAT6 targets to control alarmin responses and anti-helminth immunity. In the intestinal epithelium, the expression of GSDMC and IL-33 does not fully overlap, raising the following yet-to-be-resolved possibilities: $GSDMC_N$ pores mediating the secretion of other molecules and IL-33 being released via GSDMC-independent mechanisms. Finally, proteolytic enzymes that cleave GSDMC and mechanisms that preventing intestinal pyroptosis after $GSDMC_N$ pore formation remain to be determined.

STAR METHODS

RESOURCE AVAILABILITY

Lead Contact—Requests for further information and resources can be directed to the Lead author: Hai-Bin Ruan (hruan@umn.edu)

Materials Availability—Plasmids generated in this study are available upon request.

Data and Code Availability—RNA-seq data reported in this paper have been deposited to The Minnesota Supercomputing Institute. Original western blot images and microscopy data reported in this paper will be shared by the lead contact upon request.

This paper does not report original code.

Any additional information required to reanalyze the data reported in this paper is available from the lead contact upon request.

EXPERIMENTAL MODEL AND SUBJECT DETAILS

Animal—*Ogt-floxed* mice (Shafi et al., 2000) and *Rosa26-rOGT-floxed* mice on the C57BL/6 background were kindly provided by Dr. Xiaoyong Yang (Yang et al., 2020). *Dclk1-CreER* knockin mice were generated, validated, and kindly provided by Dr. Timothy Wang at Columbia University. *Gsdmc-floxed* mice and IEC$^{CA\text{-}STAT6\text{-}Tg}$ mice on the C57BL/6 background were generated at GemPharmatech. C57BL/6J mice (stock no. 000664), *Vil1-Cre* mice (stock no. 004586), *Il-10*$^{-/-}$ (stock no. 002251), and *Stat6*$^{-/-}$ mice (stock no. 005977) were purchased from the Jackson Laboratory. Homozygous floxed *Ogt*$^{F/F}$ mice were bred to *Vil1-Cre* and *Dclk1-CreER* mice to generate IEC$^{\Delta Ogt}$ and Tuft$^{\Delta Ogt}$ mice, respectively. Tuft$^{\Delta Ogt}$ mice and littermate controls were feed tamoxifen supplemented diet (Teklad TD. 130860) from 2 days before helminth infection until sacrifice. Homozygous floxed *Rosa26-LSL-rOGT* and *Rosa26-LSL-mOGA* mice were bred to *Vil1-Cre* mice to generate IEC$^{rOGT\text{-}Tg}$ and IEC$^{mOGA\text{-}Tg}$ mice. Whole-body *Gsdmc*$^{-/-}$ mice were generated by crossed *Gsdmc-floxed* mice to *CMV-Cre*. Cre-negative *Gsdmc*$^{-/-}$ mice were mated with *Il-10*$^{-/-}$ to generate *Gsdmc*$^{-/-}$;*Il10*$^{-/-}$ mice. All animals were kept on a 14 h: 10 h light: dark cycle in the animal facilities at the University of Minnesota, Nanjing Univeristy, and Xinxiang Medical University. Mice were group-housed unless otherwise mentioned, with free to access water and standard chow diet. All procedures involving animals were conducted within IACUC guidelines under approved protocols.

METHOD DETAILS

Helminth infection—L3 larvae of *H.polygyrus* and *N.brasiliensis* were maintained in the von Moltke laboratory and used to infect mice immediately upon arrival. *N.brasiliensis* was inoculated at the dose of 500 L3 larvae per mouse using subcutaneous injection, administered in 0.2ml PBS. *H.polygyrus* was gavaged at the dose of 200 L3 larvae per mouse in 0.1 ml of PBS.

Small intestinal epithelial cell and organoid culture—Small intestinal IECs were isolated by shaking intestinal tissue in PBS with 2 mM EDTA at 37°C for 30 min, aspirating buffer to the top of tissue and centrifugation. To isolate crypts, the EDTA-treated tissue was further shaken for 2 minutes by hands in sterile 54.9 mM D-sorbitol and 43.4 mM sucrose in PBS. Isolated crypts were filtered with 70 μm strainer, counted, and cultured in Matrigel following a published protocol (Mahe et al., 2013). Growth medium consists of Advanced DMEM/F12 with Glutamax, HEPES, Pen/Strep, 1x N2 supplement, 1x B27 supplement,

EGF (50 ng/ml), Noggin (100 ng/ml), and R-spondin conditioned media. Organoids were maintained at 37°C and medium was changed every 3 days. Cultures were split weekly by mechanical disruption of organoids. Passage 3–5 were used for experiments. Organoids were treated with 50 μM OSMI-1 or 50 ng/ml murine IL-4 for 2 days. For IL-33 secretion, isolated villus IECs and crypts were culture in DMEM with 1% FBS and Pen/Strep for 5 h. Media were collected by centrifuging at 1,500 rpm for 5 min and concentrated using Amicon Ultra-0.5 Centrifugal Filter Units (UFC500324). IL-33 concentrations were determined by Immuno blotting or ELISA (Abcam, ab213475).

Lentiviral transduction—Lentivirus was prepared by transfecting HEK293T cells with 1.5 μg pSPAX2, 0.5 μg pMD.G, and 2 μg pCDH-mSTAT6 lentiviral vector. Viral supernatant was collected for 3 consecutive days, filtered and concentrated before use. Murine intestinal organoids were infected with lentivirus based on a protocol previously described by the Hans Clevers lab with some modifications (Koo et al., 2013). Briefly, organoid media was changed to growth media plus 10 mM nicotinamide and 10μM CHIR99021 for 2 days. Then organoids were disrupted mechanically by pipetting up and down 30 to 50 times and gently dissociated enzymatically with 1X TrypLE Express at 37 °C for 3 minutes. At this stage, the organoids were ideally small clumps of < 10 cells. Organoids were then resuspended in a 24-well plate with growth media supplemented with 10 μM Y27632, 10 mM nicotinamide, 10μM CHIR99021 and 8 μg/ml Polybrene. The plate was incubated at 37 °C for 4 hours. Infected organoids were then embedded in Matrigel and cultured with growth media plus 10 μM Y27632, 10 mM nicotinamide and 10μM CHIR99021 for 3 days and then selected by 1.5μg/ml puromycin for 2 days. The survived organoids expressing mSTAT6 were transferred back to regular growth medium and expanded for experiments,

Chemicals, plasmids, transfection, and luciferase assay—ST045849 (TimTec, 20 μM) and OSMI-1 (Sigma, 50 μM) was used when indicated. The Myc-hOGT plasmid was provided by Dr. Xiaochun Yu at the University of Michigan (Chen et al., 2013). *Gsdmc2*-luc and *Pou2f3-luc* plasmids were generated by inserting the −999 to +102 bp upstream of the mouse *Gsdmc2* gene and the −1000 to +101 bp upstream of the mouse *Pou2f3* gene between the *KpnI* and *XhoI* sites of the pGL3-basic vector, respectively. STAT6 mutants were generated with the QuikChange XL II Site-Directed Mutagenesis Kit (Agilent). 293T cells were transfected with expression plasmids, luciferase reporters, and Renilla-luciferase using Lipofectamine 3000 (Invitrogen) or FuGENE HD (Promega). Cells were lysed and luciferase enzyme activities were measured using kits from Promega. Relative luciferase activity was determined by normalizing to Renilla-luc activity.

Mass spectrometry—Mouse STAT6-Myc/DDK and Myc-human OGT were co-transfected into 15cm-dishes of 293T cells and purified by immunoprecipitation with M2 Flag beads (Sigma) followed by 3xFlag peptide (Sigma) elution according to established procedures (Ruan et al., 2012). IP eluates were denatured in 0.2% Rapigest SF (Waters), reduced with 5 mM DTT, alkylated with 10 mM Iodoacetamide, and finally digested overnight at 37 °C with 5% (w:w) sequencing grade Trypsin (Promega). Digests were acidified with formic acid for 30 mins to degrade the Rapigest and peptides were then recovered and desalted with C18 OMIX tips (Agilent).

Tryptic peptides were analyzed by on-line LC-MS/MS using an Orbitrap Fusion Lumos (Thermo) coupled with a NanoAcquity UPLC system (Waters). Peptides were separated over a 15 cm × 75 μm ID 3 μm C18 EASY-Spray column (Thermo). Precursor ions were measured from 350 to 1800 m/z in the Orbitrap analyzer (resolution: 120,000; AGC: 4.0e5). Ions charged 2 + to 8 + were isolated in the quadrupole (selection window: 1.6 m/z units; dynamic exclusion window: 30 s; MIPS Peptide filter enabled), fragmented by EThcD (Maximum Injection Time: 250 ms, Normalized Collision Energy: 25%) and measured in the Orbitrap (resolution: 30,000; AGC; 5.0e4). The cycle time was 3 s.

Peaklists were generated using PAVA (UCSF) and searched using Protein Prospector 5.23.0 against the SwissProt database and a randomized concatenated database with the addition of the recombinant STAT6 sequence. Cleavage specificity was set as Trypisn allowing 2 miscleavages. Carbamidomethylation of Cys was set as a constant modification and two of the following variable modifications were allowed per peptide: acetylation of protein N-termini, oxidation of Met, oxidation and acetylation of protein N-terminal Met, cyclization of N-terminal Gln, protein N-terminal Met loss, protein N-terminal Met loss and acetylation, acetylation of Lys, phosphorylation of Ser, Thr, Tyr, HexNAc on Asn within the N glycan motif (NXST), HexNAc on Ser, Thr, Tyr, and PhosphoHexNAc on Ser or Thr. Precursor mass tolerance was 20ppm and fragment mass tolerance was 30 ppm. Phosphorylated and HexNAcylated peptides were manually verified.

Histology, immunohistochemistry, and immunofluorescence—Tissues and organoids were fixed in 10% neutral buffered formalin. Organoids were then embedded in 5% gelatin before paraffin embedding. Goblet cell staining was carried out using Alcian blue stain kit (Vector) following manufacturer's instruction. Antigen retrieval was performed in Citric buffer using a 2100 Retriever (Aptum Biologics). For immunofluorescence, tissue slides were blocked with 3% BSA, 0.2% TWEEN 20 in PBS, incubated with primary antibodies (1:100 to 1:200 dilution) overnight, and secondary antibodies (1:400 dilution) for 1h. A Nikon system was used for fluorescence detection. For cell number quantification, 3–5 random fields per sample were captured. Stained cell specifically on the epithelium were counted. In the intestine, cell number was normalized to the number of crypt/villus units (ileum) or crypts (colon). In the organoid, cell number was normalized to nuclei number as indicated by DAPI staining. For the quantification of O-GlcNAcylation intensity in intestinal epithelium, the nucleus and cytoplasm region in the epithelium were selected and quantification was performed by FIJI.

Immunoprecipitation and Immuno Blot—Tissues and cells were lysed in RIPA buffer containing proteinase inhibitors, protein phosphatase inhibitors and an OGA inhibitor. For immunoprecipitation, whole-cell lysates were incubated with and precipitated by anti-Flag beads (Millipore Sigma). Equal amounts of whole lysates or immunoprecipitation samples were electrophoresed on TGX precast gels (Bio-Rad) and transferred to nitrocellulose membrane. Membranes were incubated with primary antibodies at 4 °C for overnight. Immuno blotting was visualized by using IRDye secondary antibodies and the Odyssey imaging system (LI-COR Biosciences). Densitometry data was generated using Photoshop.

RNA and real time PCR—Total RNA was extracted from mouse tissues and organoids using TRIzol reagent (Invitrogen). cDNA was reverse transcribed (Bio-Rad) and amplified with SYBR Green Supermix (Bio-Rad) using a C1000 Thermal Cycler (Bio-Rad). All data were normalized to the expression of the *Rplp0* gene. Primer sequences are listed in Table S2.

In situ Hybridization—Intestinal tissue was processed for in situ hybridization using BaseScope™ Detection Reagent Kit v2-RED (323900, Advanced Cell Diagnostics) according to the manufacturer's protocol. The test BaseScope probes 1) BA-Mm-Gsdmc2–3-zz and 2) BA-Mm-Gsdmc4-zz were 'ZZ' antisense probes designed to targeting mouse *Gsdmc2–3* and *Gsdmc4*, respectively. The positive control probe is BA-Mm-Ppib-3zz and negative control probe: BA-Dapb-3zz.

Briefly, deparaffinized and dried sections were incubated with RNAscope® Hydrogen Peroxide for 10 min at room temperature and then 1xRNAscope® Target Retrieval Reagents for 15 min at 98~102°C. The samples were then incubated with RNAscope® Protease IV in HybEZ™ Oven (Advanced Cell Diagnostics, Hayward, CA) at 40°C for 30 min. Then each sample was hybridized with one BaseScope probe according to the requirement in HybEZ™ Oven at 40°C for 2 hours. After buffer washing steps, the samples were incubated in HybEZ™ Oven at 40°C with the serial application of BaseScope™ v2 Amp 1~8 for signal amplification. At last, Fast Red substrate was added to samples for 10 min at RT to detect target RNA and the slides were counterstained with 50% hematoxylin staining solution for 2 min at RT. Target RNA was visualized using a standard bright field microscope.

Flow cytometry—Lamina propria cells were isolated following an established protocol optimized for helminth-infected intestine tissues (Ferrer-Font et al., 2020). For surface markers, cells were stained in PBS containing 0.5% (wt/vol) BSA with relevant antibodies at 4°C for 30 min. For analysis of intracellular markers, cells were first fixed with Fixation/Permeabilization buffer (ThermoFisher, catalog no. 00-5123) at 4°C for 30 min and then stained in Permeabilization Buffer (ThermoFisher, catalog no. 00-8333) with relevant antibodies at 4°C for 30 min. Flow cytometry data were acquired on BD Fortessa X-20 and analyzed with Flowjo v10.

QUANTIFICATION AND STATISTICAL ANALYSIS

Results are shown as mean ± SEM. The comparisons were carried out using two-tailed unpaired Student's t-test, one-way ANOVA with the Dunnett *post hoc* test, and two-way ANOVA followed by post-hoc comparisons using Tukey or Bonferroni corrections.

Supplementary Material

Refer to Web version on PubMed Central for supplementary material.

Acknowledgement

We thank Dr. Timothy C. Wang, Dr. Xiaoyong Yang and Dr. Fred D. Finkelman for providing *Dclk1-CreER* mice, *Rosa26-LSL-rOGT*/*mOGA* mice and *Il4ra*$^{-/-}$ mice, respectively. We thank Dr. Reinhard Hinterleitner of University of Pittsburg for providing DNA extracted from cecum of *Tritrichomonas* colonized mice. This work was

supported by National Institute of Health (R21 AI140109, R56 AI162791, and R01 AI139420) to H.-B.R., National Natural and Science Foundation of China (U1904132) and Program for Science & Technology Innovation Talents in Higher Education of Henan Province, China (20HASTIT046) to X.X., Natural Science Foundation of Hunan Province, China (2015JJ6072 and 2020JJ4441) and Research Foundation of Education Bureau of Hunan Province, China (20A304) to K.R., Ministry of Science and Technology of China (2018YFA0801100 and 2021YFF0702100) to L.Z., National Natural Science Foundation of China (31971056) to X.G., NIH R01 DK122056 to X.S.R., NIH 1DP2AI136596 to J.v.M., and the Miriam and Sheldon G. Adelson Medical Research Foundation grant to A.L.B. H.W and N.N.J. received American Heart Association Postdoctoral Fellowship and Damon Runyon Cancer Research Foundation Fellowship (DRG-2427-21), respectively.

Reference

Allen JE, and Sutherland TE (2014). Host protective roles of type 2 immunity: parasite killing and tissue repair, flip sides of the same coin. Semin Immunol 26, 329–340. [PubMed: 25028340]

Anthony RM, Rutitzky LI, Urban JF Jr., Stadecker MJ, and Gause WC (2007). Protective immune mechanisms in helminth infection. Nat Rev Immunol 7, 975–987. [PubMed: 18007680]

Bach JF (2018). The hygiene hypothesis in autoimmunity: the role of pathogens and commensals. Nat Rev Immunol 18, 105–120. [PubMed: 29034905]

Bamias G, and Cominelli F (2015). Role of type 2 immunity in intestinal inflammation. Curr Opin Gastroenterol 31, 471–476. [PubMed: 26376478]

Banerjee A, Herring CA, Chen B, Kim H, Simmons AJ, Southard-Smith AN, Allaman MM, White JR, Macedonia MC, McKinley ET, et al. (2020). Succinate Produced by Intestinal Microbes Promotes Specification of Tuft Cells to Suppress Ileal Inflammation. Gastroenterology

Billipp TE, Nadjsombati MS, and von Moltke J (2021). Tuning tuft cells: new ligands and effector functions reveal tissue-specific function. Curr Opin Immunol 68, 98–106. [PubMed: 33166855]

Bjerknes M, Khandanpour C, Moroy T, Fujiyama T, Hoshino M, Klisch TJ, Ding Q, Gan L, Wang J, Martin MG, et al. (2012). Origin of the brush cell lineage in the mouse intestinal epithelium. Dev Biol 362, 194–218. [PubMed: 22185794]

Broz P, Pelegrin P, and Shao F (2020). The gasdermins, a protein family executing cell death and inflammation. Nat Rev Immunol 20, 143–157. [PubMed: 31690840]

Bulek K, Zhao J, Liao Y, Rana N, Corridoni D, Antanaviciute A, Chen X, Wang H, Qian W, Miller-Little WA, et al. (2020). Epithelial-derived gasdermin D mediates nonlytic IL-1beta release during experimental colitis. J Clin Invest 130, 4218–4234. [PubMed: 32597834]

Camberis M, Le Gros G, and Urban J Jr. (2003). Animal model of Nippostrongylus brasiliensis and Heligmosomoides polygyrus. Curr Protoc Immunol Chapter 19, Unit 19 12.

Cayrol C, Duval A, Schmitt P, Roga S, Camus M, Stella A, Burlet-Schiltz O, Gonzalez-de-Peredo A, and Girard JP (2018). Environmental allergens induce allergic inflammation through proteolytic maturation of IL-33. Nat Immunol 19, 375–385. [PubMed: 29556000]

Cayrol C, and Girard JP (2018). Interleukin-33 (IL-33): A nuclear cytokine from the IL-1 family. Immunol Rev 281, 154–168. [PubMed: 29247993]

Chang YH, Weng CL, and Lin KI (2020). O-GlcNAcylation and its role in the immune system. J Biomed Sci 27, 57. [PubMed: 32349769]

Chao KL, Kulakova L, and Herzberg O (2017). Gene polymorphism linked to increased asthma and IBD risk alters gasdermin-B structure, a sulfatide and phosphoinositide binding protein. Proc Natl Acad Sci U S A 114, E1128–E1137. [PubMed: 28154144]

Chen Q, Chen Y, Bian C, Fujiki R, and Yu X (2013). TET2 promotes histone O-GlcNAcylation during gene transcription. Nature 493, 561–564. [PubMed: 23222540]

Das S, Miller M, Beppu AK, Mueller J, McGeough MD, Vuong C, Karta MR, Rosenthal P, Chouiali F, Doherty TA, et al. (2016). GSDMB induces an asthma phenotype characterized by increased airway responsiveness and remodeling without lung inflammation. Proc Natl Acad Sci U S A 113, 13132–13137. [PubMed: 27799535]

Das S, Miller M, and Broide DH (2017). Chromosome 17q21 Genes ORMDL3 and GSDMB in Asthma and Immune Diseases. Adv Immunol 135, 1–52. [PubMed: 28826527]

Diefenbach A, Gnafakis S, and Shomrat O (2020). Innate Lymphoid Cell-Epithelial Cell Modules Sustain Intestinal Homeostasis. Immunity 52, 452–463. [PubMed: 32187516]

Ferrer-Font L, Mehta P, Harmos P, Schmidt AJ, Chappell S, Price KM, Hermans IF, Ronchese F, le Gros G, and Mayer JU (2020). High-dimensional analysis of intestinal immune cells during helminth infection. Elife 9.

Gerbe F, Sidot E, Smyth DJ, Ohmoto M, Matsumoto I, Dardalhon V, Cesses P, Garnier L, Pouzolles M, Brulin B, et al. (2016). Intestinal epithelial tuft cells initiate type 2 mucosal immunity to helminth parasites. Nature 529, 226–230. [PubMed: 26762460]

Gewinner C, Hart G, Zachara N, Cole R, Beisenherz-Huss C, and Groner B (2004). The coactivator of transcription CREB-binding protein interacts preferentially with the glycosylated form of Stat5. J Biol Chem 279, 3563–3572. [PubMed: 14597631]

Gingras S, Simard J, Groner B, and Pfitzner E (1999). p300/CBP is required for transcriptional induction by interleukin-4 and interacts with Stat6. Nucleic Acids Res 27, 2722–2729. [PubMed: 10373589]

Hanover JA, Krause MW, and Love DC (2012). Bittersweet memories: linking metabolism to epigenetics through O-GlcNAcylation. Nat Rev Mol Cell Biol 13, 312–321. [PubMed: 22522719]

Hardiville S, and Hart GW (2014). Nutrient regulation of signaling, transcription, and cell physiology by O-GlcNAcylation. Cell Metab 20, 208–213. [PubMed: 25100062]

Harnik Y, Buchauer L, Ben-Moshe S, Averbukh I, Levin Y, Savidor A, Eilam R, Moor AE, and Itzkovitz S (2021). Spatial discordances between mRNAs and proteins in the intestinal epithelium. Nature Metabolism 3, 1680–1693.

Harris NL, and Loke P (2017). Recent Advances in Type-2-Cell-Mediated Immunity: Insights from Helminth Infection. Immunity 47, 1024–1036. [PubMed: 29262347]

Hodzic Z, Schill EM, Bolock AM, and Good M (2017). IL-33 and the intestine: The good, the bad, and the inflammatory. Cytokine 100, 1–10. [PubMed: 28687373]

Hou J, Zhao R, Xia W, Chang CW, You Y, Hsu JM, Nie L, Chen Y, Wang YC, Liu C, et al. (2020). PD-L1-mediated gasdermin C expression switches apoptosis to pyroptosis in cancer cells and facilitates tumour necrosis. Nat Cell Biol

Howitt MR, Lavoie S, Michaud M, Blum AM, Tran SV, Weinstock JV, Gallini CA, Redding K, Margolskee RF, Osborne LC, et al. (2016). Tuft cells, taste-chemosensory cells, orchestrate parasite type 2 immunity in the gut. Science 351, 1329–1333. [PubMed: 26847546]

Hung LY, Lewkowich IP, Dawson LA, Downey J, Yang Y, Smith DE, and Herbert DR (2013). IL-33 drives biphasic IL-13 production for noncanonical Type 2 immunity against hookworms. Proc Natl Acad Sci U S A 110, 282–287. [PubMed: 23248269]

Hung LY, Tanaka Y, Herbine K, Pastore C, Singh B, Ferguson A, Vora N, Douglas B, Zullo K, Behrens EM, et al. (2020). Cellular context of IL-33 expression dictates impact on anti-helminth immunity. Sci Immunol 5.

Kamal M, Dehlawi MS, Brunet LR, and Wakelin D (2002). Paneth and intermediate cell hyperplasia induced in mice by helminth infections. Parasitology 125, 275–281. [PubMed: 12358424]

Khan WI, Blennerhasset P, Ma C, Matthaei KI, and Collins SM (2001). Stat6 dependent goblet cell hyperplasia during intestinal nematode infection. Parasite Immunol 23, 39–42. [PubMed: 11136476]

Koo BK, Sasselli V, and Clevers H (2013). Retroviral gene expression control in primary organoid cultures. Curr Protoc Stem Cell Biol 27, Unit 5A 6.

Kouzaki H, Iijima K, Kobayashi T, O'Grady SM, and Kita H (2011). The danger signal, extracellular ATP, is a sensor for an airborne allergen and triggers IL-33 release and innate Th2-type responses. J Immunol 186, 4375–4387. [PubMed: 21357533]

Kuhn R, Lohler J, Rennick D, Rajewsky K, and Muller W (1993). Interleukin-10-deficient mice develop chronic enterocolitis. Cell 75, 263–274. [PubMed: 8402911]

Lei W, Ren W, Ohmoto M, Urban JF Jr., Matsumoto I, Margolskee RF, and Jiang P (2018). Activation of intestinal tuft cell-expressed Sucnr1 triggers type 2 immunity in the mouse small intestine. Proc Natl Acad Sci U S A 115, 5552–5557. [PubMed: 29735652]

Liu B, Salgado OC, Singh S, Hippen KL, Maynard JC, Burlingame AL, Ball LE, Blazar BR, Farrar MA, Hogquist KA, et al. (2019). The lineage stability and suppressive program of regulatory T cells require protein O-GlcNAcylation. Nat Commun 10, 354. [PubMed: 30664665]

Liu J, Qian C, and Cao X (2016). Post-Translational Modification Control of Innate Immunity. Immunity 45, 15–30. [PubMed: 27438764]

Lloyd CM, and Snelgrove RJ (2018). Type 2 immunity: Expanding our view. Sci Immunol 3.

Ma C, Yang D, Wang B, Wu C, Wu Y, Li S, Liu X, Lassen K, Dai L, and Yang S (2020). Gasdermin D in macrophages restrains colitis by controlling cGAS-mediated inflammation. Sci Adv 6, eaaz6717. [PubMed: 32671214]

Mahe MM, Aihara E, Schumacher MA, Zavros Y, Montrose MH, Helmrath MA, Sato T, and Shroyer NF (2013). Establishment of Gastrointestinal Epithelial Organoids. Curr Protoc Mouse Biol 3, 217–240. [PubMed: 25105065]

Maiti NR, Sharma P, Harbor PC, and Haque SJ (2005). Serine phosphorylation of Stat6 negatively controls its DNA-binding function. J Interferon Cytokine Res 25, 553–563. [PubMed: 16181056]

Martinez MR, Dias TB, Natov PS, and Zachara NE (2017). Stress-induced O-GlcNAcylation: an adaptive process of injured cells. Biochem Soc Trans 45, 237–249. [PubMed: 28202678]

McGinty JW, Ting HA, Billipp TE, Nadjsombati MS, Khan DM, Barrett NA, Liang HE, Matsumoto I, and von Moltke J (2020). Tuft-Cell-Derived Leukotrienes Drive Rapid Anti-helminth Immunity in the Small Intestine but Are Dispensable for Anti-protist Immunity. Immunity 52, 528–541 e527. [PubMed: 32160525]

Mikita T, Campbell D, Wu P, Williamson K, and Schindler U (1996). Requirements for interleukin-4-induced gene expression and functional characterization of Stat6. Mol Cell Biol 16, 5811–5820. [PubMed: 8816495]

Molodecky NA, Soon IS, Rabi DM, Ghali WA, Ferris M, Chernoff G, Benchimol EI, Panaccione R, Ghosh S, Barkema HW, et al. (2012). Increasing incidence and prevalence of the inflammatory bowel diseases with time, based on systematic review. Gastroenterology 142, 46–54 e42; quiz e30. [PubMed: 22001864]

Morita H, Nakae S, Saito H, and Matsumoto K (2017). IL-33 in clinical practice: Size matters? J Allergy Clin Immunol 140, 381–383. [PubMed: 28478050]

Nadjsombati MS, McGinty JW, Lyons-Cohen MR, Jaffe JB, DiPeso L, Schneider C, Miller CN, Pollack JL, Nagana Gowda GA, Fontana MF, et al. (2018). Detection of Succinate by Intestinal Tuft Cells Triggers a Type 2 Innate Immune Circuit. Immunity 49, 33–41 e37. [PubMed: 30021144]

O'Grady SM, Patil N, Melkamu T, Maniak PJ, Lancto C, and Kita H (2013). ATP release and Ca2+ signalling by human bronchial epithelial cells following Alternaria aeroallergen exposure. J Physiol 591, 4595–4609. [PubMed: 23858006]

Oliphant CJ, Barlow JL, and McKenzie ANJ (2011). Insights into the initiation of type 2 immune responses. Immunology 134, 378–385. [PubMed: 22044021]

Pastille E, Frede A, McSorley HJ, Grab J, Adamczyk A, Kollenda S, Hansen W, Epple M, Buer J, Maizels RM, et al. (2017). Intestinal helminth infection drives carcinogenesis in colitis-associated colon cancer. PLoS Pathog 13, e1006649. [PubMed: 28938014]

Qin W, Lv P, Fan X, Quan B, Zhu Y, Qin K, Chen Y, Wang C, and Chen X (2017). Quantitative time-resolved chemoproteomics reveals that stable O-GlcNAc regulates box C/D snoRNP biogenesis. Proc Natl Acad Sci U S A 114, E6749–E6758. [PubMed: 28760965]

Rana N, Privitera G, Kondolf HC, Bulek K, Lechuga S, De Salvo C, Corridoni D, Antanaviciute A, Maywald RL, Hurtado AM, et al. (2022). GSDMB is increased in IBD and regulates epithelial restitution/repair independent of pyroptosis. Cell

Ribet D, and Cossart P (2010). Pathogen-mediated posttranslational modifications: A re-emerging field. Cell 143, 694–702. [PubMed: 21111231]

Ruan HB, Dietrich MO, Liu ZW, Zimmer MR, Li MD, Singh JP, Zhang K, Yin R, Wu J, Horvath TL, et al. (2014). O-GlcNAc transferase enables AgRP neurons to suppress browning of white fat. Cell 159, 306–317. [PubMed: 25303527]

Ruan HB, Han X, Li MD, Singh JP, Qian K, Azarhoush S, Zhao L, Bennett AM, Samuel VT, Wu J, et al. (2012). O-GlcNAc transferase/host cell factor C1 complex regulates gluconeogenesis by modulating PGC-1alpha stability. Cell Metab 16, 226–237. [PubMed: 22883232]

Ruan HB, Ma Y, Torres S, Zhang B, Feriod C, Heck RM, Qian K, Fu M, Li X, Nathanson MH, et al. (2017). Calcium-dependent O-GlcNAc signaling drives liver autophagy in adaptation to starvation. Genes Dev 31, 1655–1665. [PubMed: 28903979]

Ruan HB, Nie Y, and Yang X (2013a). Regulation of protein degradation by O-GlcNAcylation: crosstalk with ubiquitination. Mol Cell Proteomics 12, 3489–3497. [PubMed: 23824911]

Ruan HB, Singh JP, Li MD, Wu J, and Yang X (2013b). Cracking the O-GlcNAc code in metabolism. Trends Endocrinol Metab 24, 301–309. [PubMed: 23647930]

Schneider C, O'Leary CE, and Locksley RM (2019). Regulation of immune responses by tuft cells. Nat Rev Immunol 19, 584–593. [PubMed: 31114038]

Schneider C, O'Leary CE, von Moltke J, Liang HE, Ang QY, Turnbaugh PJ, Radhakrishnan S, Pellizzon M, Ma A, and Locksley RM (2018). A MetaboliteTriggered Tuft Cell-ILC2 Circuit Drives Small Intestinal Remodeling. Cell 174, 271–284 e214. [PubMed: 29887373]

Schubart C, Krljanac B, Otte M, Symowski C, Martini E, Gunther C, Becker C, Daniel C, and Voehringer D (2019). Selective expression of constitutively activated STAT6 in intestinal epithelial cells promotes differentiation of secretory cells and protection against helminths. Mucosal Immunol 12, 413–424. [PubMed: 30446727]

Schuijers J, van der Flier LG, van Es J, and Clevers H (2014). Robust cre-mediated recombination in small intestinal stem cells utilizing the olfm4 locus. Stem Cell Reports 3, 234–241. [PubMed: 25254337]

Shafi R, Iyer SP, Ellies LG, O'Donnell N, Marek KW, Chui D, Hart GW, and Marth JD (2000). The O-GlcNAc transferase gene resides on the X chromosome and is essential for embryonic stem cell viability and mouse ontogeny. Proc Natl Acad Sci U S A 97, 5735–5739. [PubMed: 10801981]

Smallwood TB, Giacomin PR, Loukas A, Mulvenna JP, Clark RJ, and Miles JJ (2017). Helminth Immunomodulation in Autoimmune Disease. Front Immunol 8, 453. [PubMed: 28484453]

Srisomboon Y, Squillace DL, Maniak PJ, Kita H, and O'Grady SM (2020). Fungal allergen-induced IL-33 secretion involves cholesterol-dependent, VDAC-1-mediated ATP release from the airway epithelium. J Physiol 598, 1829–1845. [PubMed: 32103508]

Stockinger S, Albers T, Duerr CU, Menard S, Putsep K, Andersson M, and Hornef MW (2014). Interleukin-13-mediated paneth cell degranulation and antimicrobial peptide release. J Innate Immun 6, 530–541. [PubMed: 24556597]

Su C, Su L, Li Y, Long SR, Chang J, Zhang W, Walker WA, Xavier RJ, Cherayil BJ, and Shi HN (2018). Helminth-induced alterations of the gut microbiota exacerbate bacterial colitis. Mucosal Immunol 11, 144–157. [PubMed: 28352104]

Ting HA, and von Moltke J (2019). The Immune Function of Tuft Cells at Gut Mucosal Surfaces and Beyond. J Immunol 202, 1321–1329. [PubMed: 30782851]

Uchida M, Anderson EL, Squillace DL, Patil N, Maniak PJ, Iijima K, Kita H, and O'Grady SM (2017). Oxidative stress serves as a key checkpoint for IL-33 release by airway epithelium. Allergy 72, 1521–1531. [PubMed: 28273344]

Varyani F, Fleming JO, and Maizels RM (2017). Helminths in the gastrointestinal tract as modulators of immunity and pathology. American Journal of Physiology-Gastrointestinal and Liver Physiology 312, G537–G549. [PubMed: 28302598]

von Moltke J, Ji M, Liang HE, and Locksley RM (2016). Tuft-cell-derived IL-25 regulates an intestinal ILC2-epithelial response circuit. Nature 529, 221–225. [PubMed: 26675736]

Wang Y, Malabarba MG, Nagy ZS, and Kirken RA (2004). Interleukin 4 regulates phosphorylation of serine 756 in the transactivation domain of Stat6. Roles for multiple phosphorylation sites and Stat6 function. J Biol Chem 279, 25196–25203. [PubMed: 15069079]

Westphalen CB, Asfaha S, Hayakawa Y, Takemoto Y, Lukin DJ, Nuber AH, Brandtner A, Setlik W, Remotti H, Muley A, et al. (2014). Long-lived intestinal tuft cells serve as colon cancer-initiating cells. J Clin Invest 124, 1283–1295. [PubMed: 24487592]

Whelan SA, Lane MD, and Hart GW (2008). Regulation of the O-linked beta-Nacetylglucosamine transferase by insulin signaling. J Biol Chem 283, 21411–21417. [PubMed: 18519567]

Williams MA, O'Callaghan A, and Corr SC (2019). IL-33 and IL-18 in Inflammatory Bowel Disease Etiology and Microbial Interactions. Front Immunol 10, 1091. [PubMed: 31139196]

Wynn TA (2015). Type 2 cytokines: mechanisms and therapeutic strategies. Nat Rev Immunol 15, 271–282. [PubMed: 25882242]

Xi R, Montague J, Lin X, Lu C, Lei W, Tanaka K, Zhang YV, Xu X, Zheng X, Zhou X, et al. (2021). Up-regulation of gasdermin C in mouse small intestine is associated with lytic cell death in enterocytes in worm-induced type 2 immunity. Proc Natl Acad Sci U S A 118.

Yang X, and Qian K (2017). Protein O-GlcNAcylation: emerging mechanisms and functions. Nat Rev Mol Cell Biol 18, 452–465. [PubMed: 28488703]

Yang Y, Fu M, Li MD, Zhang K, Zhang B, Wang S, Liu Y, Ni W, Ong Q, Mi J, et al. (2020). O-GlcNAc transferase inhibits visceral fat lipolysis and promotes diet-induced obesity. Nat Commun 11, 181. [PubMed: 31924761]

Yazdanbakhsh M, Kremsner PG, and van Ree R (2002). Allergy, parasites, and the hygiene hypothesis. Science 296, 490–494. [PubMed: 11964470]

Zhang JY, Zhou B, Sun RY, Ai YL, Cheng K, Li FN, Wang BR, Liu FJ, Jiang ZH, Wang WJ, et al. (2021). The metabolite α-KG induces GSDMC-dependent pyroptosis through death receptor 6-activated caspase-8. Cell Res

Zhao M, Ren K, Xiong X, Cheng M, Zhang Z, Huang Z, Han X, Yang X, Alejandro EU, and Ruan HB (2020). Protein O-GlcNAc Modification Links Dietary and Gut Microbial Cues to the Differentiation of Enteroendocrine L Cells. Cell Rep 32, 108013. [PubMed: 32783937]

Zhao M, Xiong X, Ren K, Xu B, Cheng M, Sahu C, Wu K, Nie Y, Huang Z, Blumberg RS, et al. (2018). Deficiency in intestinal epithelial O-GlcNAcylation predisposes to gut inflammation. EMBO Mol Med 10.

Zhao W, and Hu Z (2010). The enigmatic processing and secretion of interleukin-33. Cell Mol Immunol 7, 260–262. [PubMed: 20305685]

Highlights

- Helminth infection-induced O-GlcNAcylation activates epithelial STAT6 signaling.
- STAT6 O-GlcNAcylation promotes *Pou2f3* transcription and Tuft cell differentiation.
- STAT6 O-GlcNAcylation enables IL-33 secretion from $GSDMC_N$ pores.
- GSDMC activation drives anti-helminth responses and intestinal inflammation.

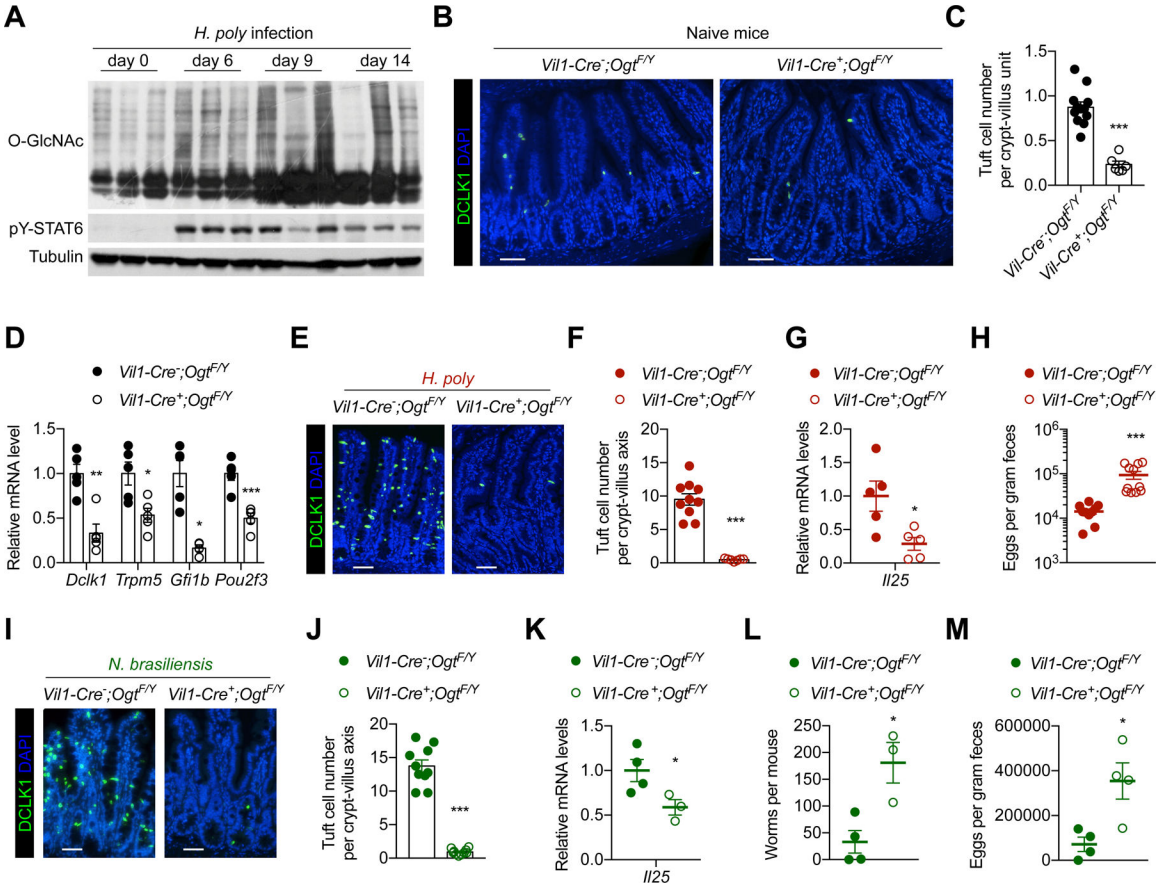

Figure 1. Defective tuft cell hyperplasia and anti-helminth activity in IEC$^{\Delta Ogt}$ mice.

(**A**) Intestinal O-GlcNAcylation and pY-STAT6 post *H. polygyrus* infection (n = 3).

(**B, C**) Immunostaining (B) and quantification (C) of tuft cells in the small intestine (SI) of naïve wildtype (n = 12) and IEC$^{\Delta Ogt}$ mice (n = 6).

(**D**) Expression of tuft cell marker genes in the IECs from naïve mice (n = 5).

(**E, F**) Immunostaining (E) and quantification (F) of SI tuft cells (n = 7–10) at 14 days post-infection (dpi).

(**G**) SI *Il25* gene expression (n = 5).

(**H**) Enumeration of worm eggs in the feces (n = 10–11).

(**I-M**) Control (n = 4–10) and IEC$^{\Delta Ogt}$ mice (n = 3–10) were infected with *N. brasiliensis* for 7 days. Tuft cells were stained (I) and then quantified (J). *Il25* gene expression was determined (K). Live adult worms in the intestinal (L) and fecal eggs (M) were enumerated. Data are represented as mean ± SEM. * P < 0.05, ** P < 0.01, *** P < 0.001 by two-tailed unpaired Student's t-test. Scale bar = 50 μm. Please also see Figure S1.

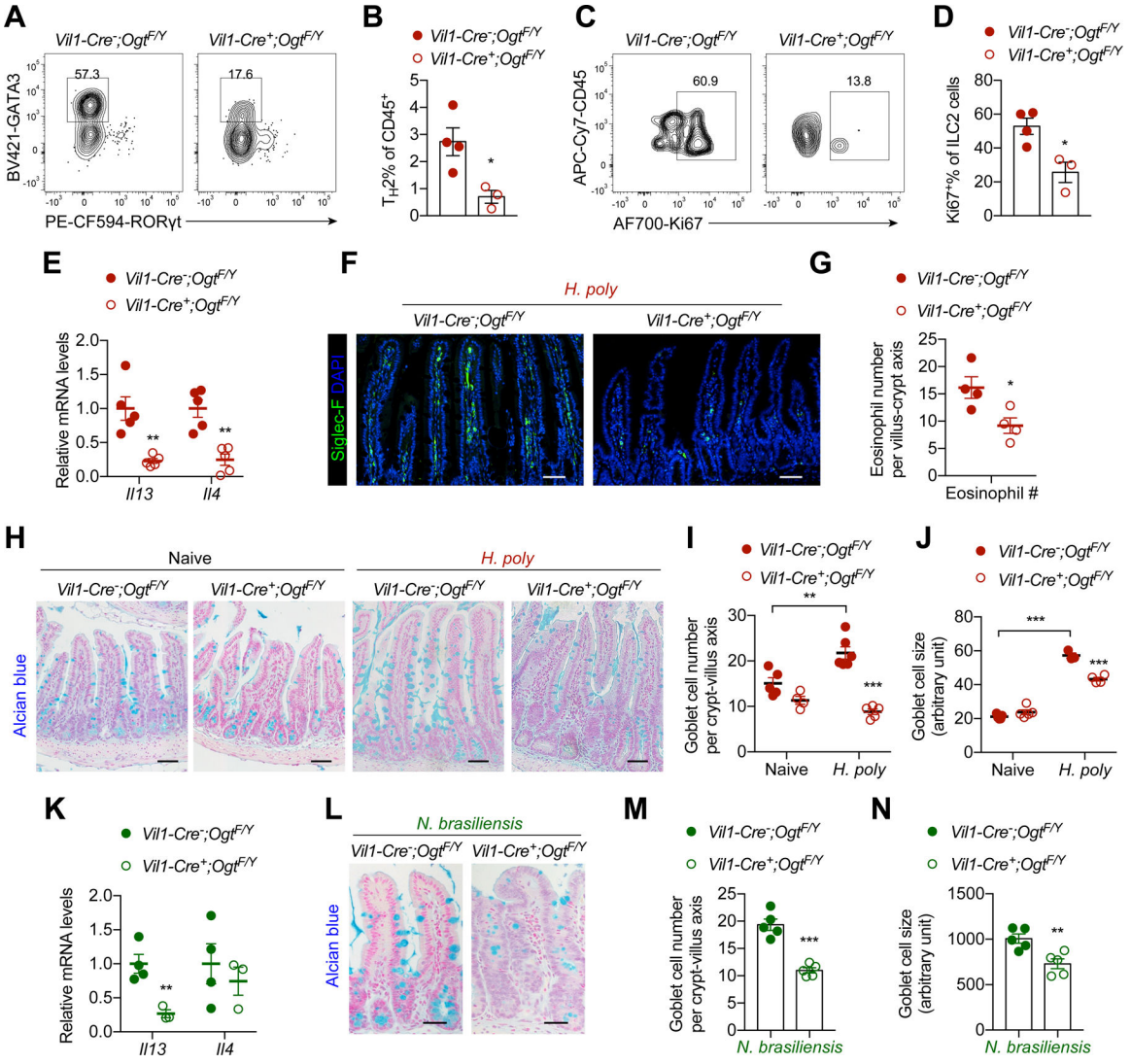

Figure 2. Defective. Defective type 2 immune responses and goblet cell hyperplasia in IEC$^{\Delta Ogt}$ mice.

(**A,B**) Flow cytometry of GATA3^{+} Th2 cells among non-Treg CD4 T cells (A) and frequencies of Th2 cells among CD45^{+} cells (B, n = 3–4) in the SI lamina propria of *H. polygyrus*-infected mice.

(**C, D**) Flow cytometry (C) and percentage (D, n = 3–4) of Ki67^{+} ILC2 cells in the SI lamina propria of *H. polygyrus*-infected mice.

(**E**) *Il13* and *Il4* expression in the SI of *H. polygyrus*-infected mice (n = 5).

(**F, G**) Immunostaining (F) and quantification (G) of Siglec-F^{+} eosinophils in the SI of *H. polygyrus*-infected mice (n = 4).

(**H-J**) Alcian blue staining of the SI of *H. polygyrus*-infected mice (H). Goblet cell number (I) and size (J) were quantified (n = 4–6).

(**K-N**) Mice were infected with *N. brasiliensis*. *Il13* and *Il4* gene expression was determined (K, n = 3–4). Goblet cells were stained with Alcian blue (L, n = 5) and their number (M) and size (N) were quantified.

Data are represented as mean ± SEM. * $P < 0.05$, ** $P < 0.01$, *** $P < 0.001$ by two-way ANOVA (I, J) or two-tailed unpaired Student's t-test. Scale bar = 50 μm. Please also see Figure S2.

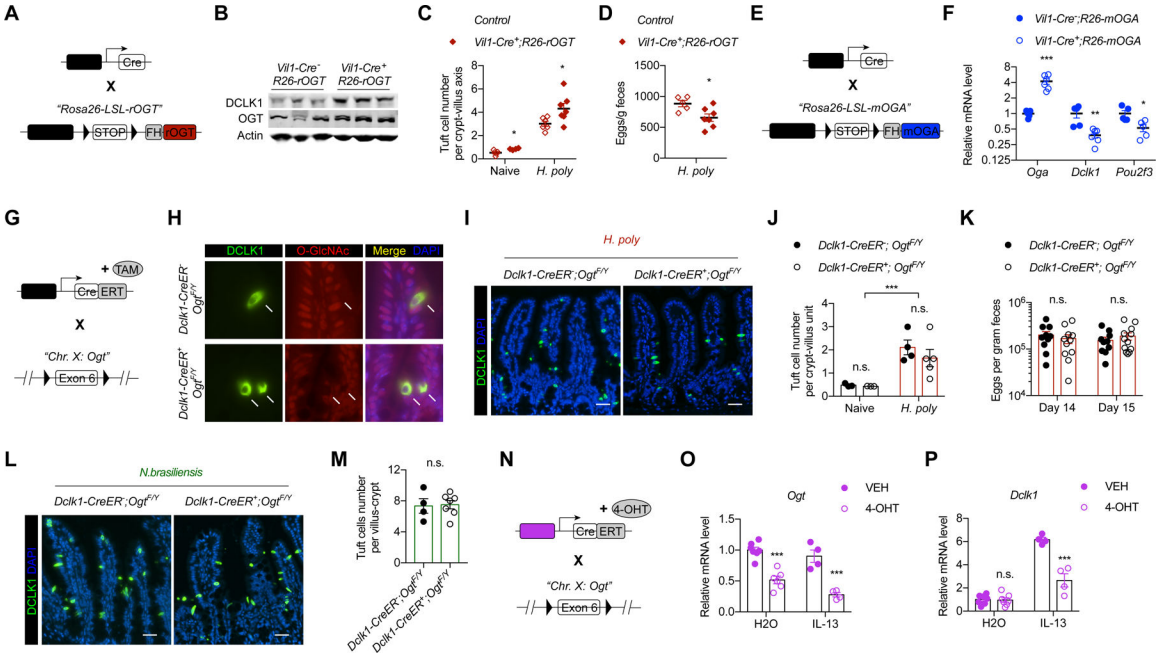

Figure 3. OGT in mature tuft cells is dispensable for antihelminth responses.

(**A,B**) Generation (A) and validation (B) of OGT overexpression in mouse intestinal epithelium.

(**C, D**) *H. polygyrus*-infected mice (n = 5–7) were sacrificed for SI tuft cell quantification (C) and fecal worm egg enumeration (D).

(**E, F**) IEC$^{mOGA\text{-}Tg}$ mice were generated (E) and expression of tuft cell markers was determined (F, n = 5–6).

(**G**) Generation of Tuft$^{\Delta Ogt}$ mice.

(**H**) Validation of O-GlcNAc depletion by immunostaining in DCLK1^{+} tuft cells of Tuft$^{\Delta Ogt}$ mice.

(**I-K**) Tamoxifen-fed control and Tuft$^{\Delta Ogt}$ mice were infected with *H. polygyrus*. DCLK1 staining (**I**) and quantification (J, n = 3–5) of SI tuft cells. Enumeration of fecal worm eggs (L, n = 10–12).

(**L, M**) Control (n = 4) and Tuft$^{\Delta Ogt}$ (n = 7) mice were infected with *N. brasiliensis*. SI tuft cells were stained (L) and quantified (M).

(**N-P**) ISC$^{\Delta Ogt}$ mice were generated (N) and SI organoids (n = 4) were treated with 4-OHT to induce *Ogt* deletion (O). Expression of the *Dclk1* gene was determined (P)

Data are represented as mean ± SEM. * P < 0.05, ** P < 0.01, *** P < 0.001 by two-way ANOVA (J, O, P) and two-tailed unpaired Student's t-test. n.s., not significant. Scale bar = 50 μm. Please also see Figure S3.

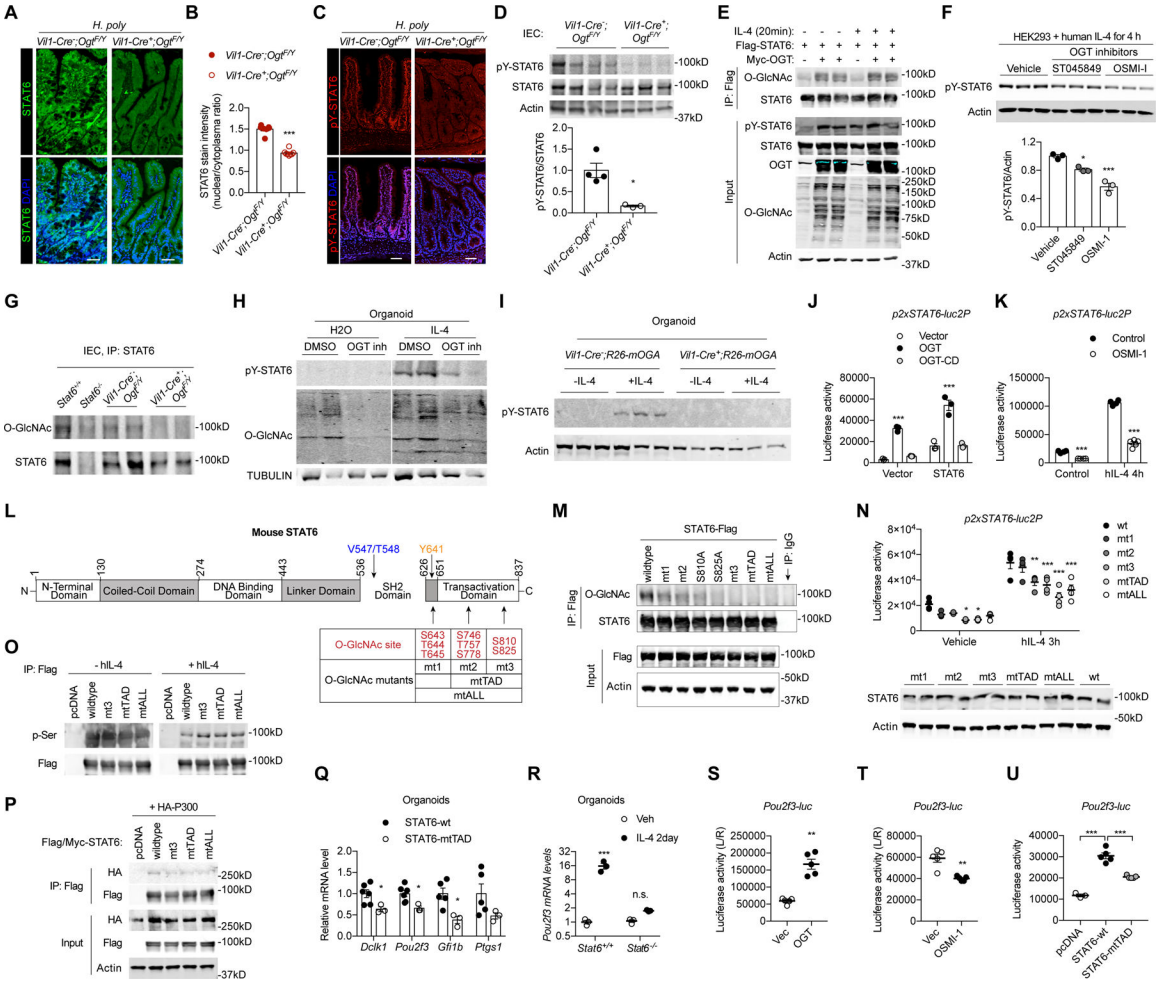

Figure 4. STAT6 O-GlcNAcylation promotes *Pou2f3* transcription.

(**A,B**) STAT6 immunostaining (A) and ratio of nuclear vs. cytoplasmic fluorescent intensity (B) in SI from *H. polygyrus*-infected mice (n = 7–8).

(**C, D**) pY-STAT6 immunostaining (C) and immunoblotting (D) in SI epithelial cells from *H. polygyrus*-infected mice (n = 3–4).

(**E**) HEK 293 cells were transfected and treated with human IL-4 for 20 min. Whole cell lysate and STAT6 immunoprecipitation were immunoblotted.

(**F**) HEK 293 cells were pre-treated with OGT inhibitors overnight, stimulated with human IL-4 for 4 hours, and subjected to immunoblotting.

(**G**) IEC protein from *Stat6*$^{-/-}$, IEC$^{\Delta Ogt}$ and their controls was subjected to STAT6 immunoprecipitation, followed by immunoblotting with an anti-O-GlcNAc antibody.

(**H**) SI organoids were pre-treated with an OGT inhibitor overnight, stimulated with murine IL-4, and subjected to pY-STAT6 and O-GlcNAc immunoblotting.

(**I**) SI organoids from control and IEC$^{mOGA\text{-}Tg}$ mice were treated with or without IL-4, and subjected to pY-STAT6 immunoblotting.

(**J, K**) *p2xSTAT6-Luc2P* luciferase reporter assays in HEK 293 cells co-transfected with OGT and STAT6 (E, n = 3) or treated with OGT inhibitor and IL-4 (F, n = 4–5).

(**L**) Structural domains of mouse STAT6. Red: O-GlcNAc sites; Green, pY site; Blue, sites critical for dimerization.
(**M**) Flag-tagged STAT6 mutants were expressed in HEK 293 cells, immunoprecipitated, and immunoblotted for O-GlcNAcylation.
(**N**) *p2xSTAT6-Luc2P* luciferase reporter assays in HEK 293 transfected with STAT6 plasmids, followed with IL-4 stimulation (top). Equal expression of STAT6 proteins was shown (bottom).
(**O**) Flag-tagged STAT6 mutants were expressed in HEK 293 cells, treated with human IL-4, immunoprecipitated, and immunoblotted with a pan phospho-Serine antibody.
(**P**) Flag-tagged STAT6 mutants and HA-tagged P300 were expressed in HEK 293 cells. Co-immunoprecipitated was done with an anti-Flag antibody and determined by HA immunoblotting.
(**Q**) SI organoids were transduced with lentiviruses expressing wildtype (n = 6) or mtTAD (n = 3) STAT6, stimulated with IL-4 for 2 days, and subjected to RT-qPCR of tuft cell markers.
(**R**) *Pou2f3* gene expression in $Stat6^{+/+}$ or $Stat6^{-/-}$ organoids treated with IL-4 for 2 days (n = 3).
(**S-U**) Luciferase of the *Pou2f3* promoter in the presence of OGT overexpression (S, n = 5), the OGT inhibitor OSMI-1 (T, n =5), or WT/mtTAD-STAT6 (U, n = 4).
Data are represented as mean ± SEM. * $P < 0.05$, ** $P < 0.01$, *** $P < 0.001$ by one-way ANOVA (F, U), two-way ANOVA (J, K, R), or two-tailed unpaired Student's t-test. Scale bar = 50 μm. Please also see Figure S4.

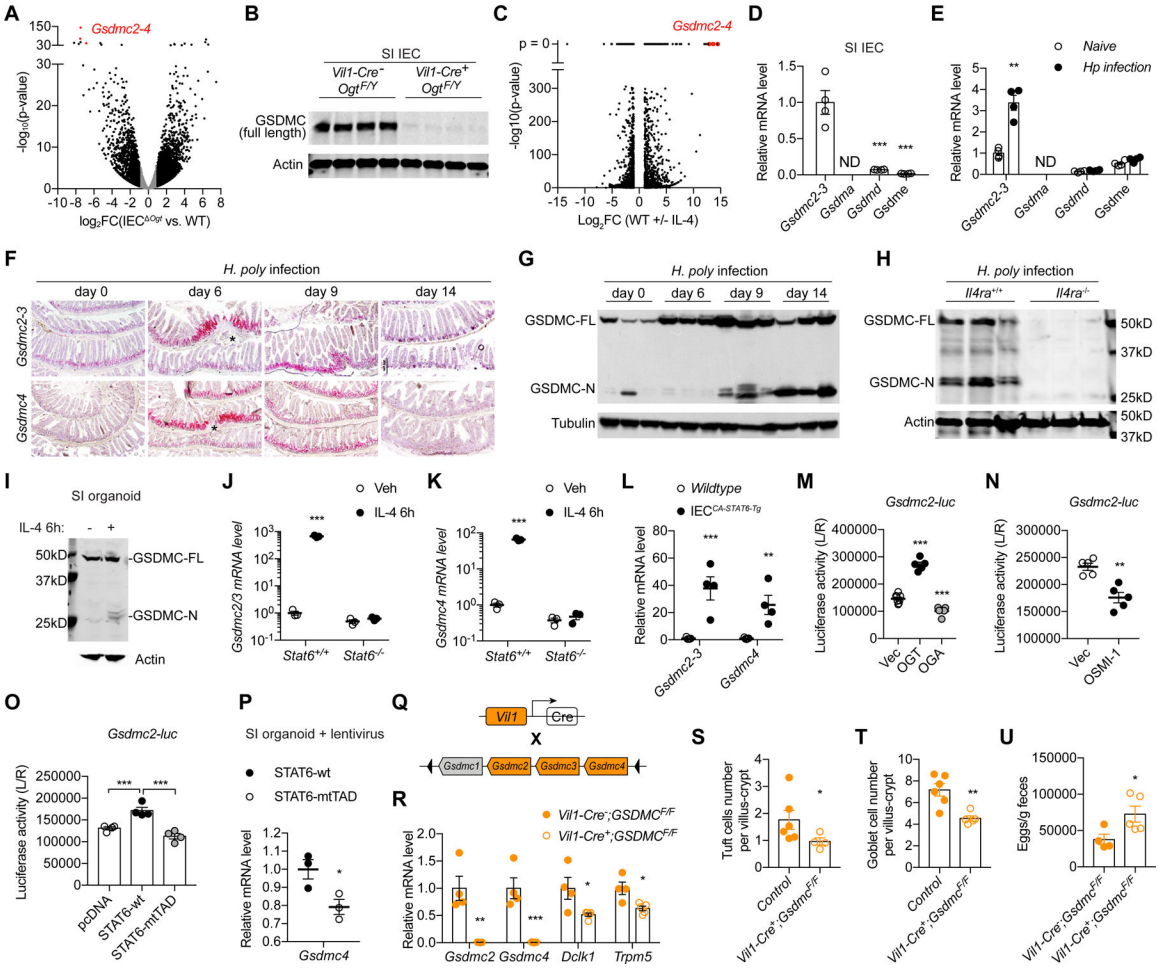

Figure 5. Intestinal epithelial *Gsdmc* transcription is dictated by OGT and STAT6 O-GlcNAcylation.

(**A**) Volcano plot showing differentially expressed gene in SI IECs in IEC$^{\Delta Ogt}$ vs. wildtype mice. *Gsdmc2–4* genes were highlighted in red.

(**B**)Amounts of GSDMC protein (n = 4) in the SI of wildtype and IEC$^{\Delta Ogt}$ mice.

(**C**) Volcano plot showing differentially expressed gene in SI organoids with vs. without IL-4 treatment. *Gsdmc2–4* genes were highlighted in red.

(**D, E**) Relative expression of Gasdermin family genes in SI IECs (D, n = 4) and in the SI from naive vs. *H. polygyrus*-infected mice (F, n = 4).

(**F**) In situ hybridization of *Gsdmc2–3* (top) and *Gsdmc4* (bottom) mRNA in the SI from mice after *H. polygyrus* infection (n = 3). * denotes granuloma. Scale bar = 200 μm.

(**G-I**) Expression of full length (FL) and N-terminal GSDMC in the SI post *H. polygyrus* infection (G, n = 3), SI IECs from infected *Il4ra*$^{+/+}$ and *Il4ra*$^{-/-}$ mice (H, n = 3), and in SI organoids treated with or without IL-4 for 6 h (I). The same Tubulin blot in Figure 1A was used in (G) for the loading control.

(**J, K**) *Gsdmc2–3* (J) and *Gsdmc4* (K) expression in *Stat6*$^{+/+}$ and *Stat6*$^{-/-}$ organoids treated with IL-4 for 2 days (n = 3).

(**L**) SI *Gsdmc2–3* and *Gsdmc4* expression in wildtype (n = 5) and IEC$^{CA\text{-}STAT6\text{-}Tg}$ (n = 4) mice.

(**M-O**) Luciferase of the *Gsdmc2* promoter in HEK 293 cells in the presence of OGT and OGA overexpression (M, n = 5), the OGT inhibitor OSMI-1 (N, n =5), or WT/mtTAD-STAT6 (O, n = 4).

(**P**) SI organoids were transduced with lentiviral STAT6 (n = 3). Endogenous *Gsdmc4* gene expression was determined. (**Q**) Generation of $IEC^{\Delta Gsdmc}$ mice.

(**R-S**) Mice were infected with *H. polygyrus*. (R) Tuft cell marker gene expression (n = 4–5). (S) Quantification of tuft cell number (n = 4–6). (T) Alcian staining and quantification of goblet cells (n = 4–6). (U) Enumeration of fecal worm eggs (n = 4–5).

Data are represented as mean ± SEM. * $P < 0.05$, ** $P < 0.01$, *** $P < 0.001$ by one-way ANOVA (D, M, O), two-way ANOVA (J, K) or two-tailed unpaired Student's t-test. Please also see Figure S5.

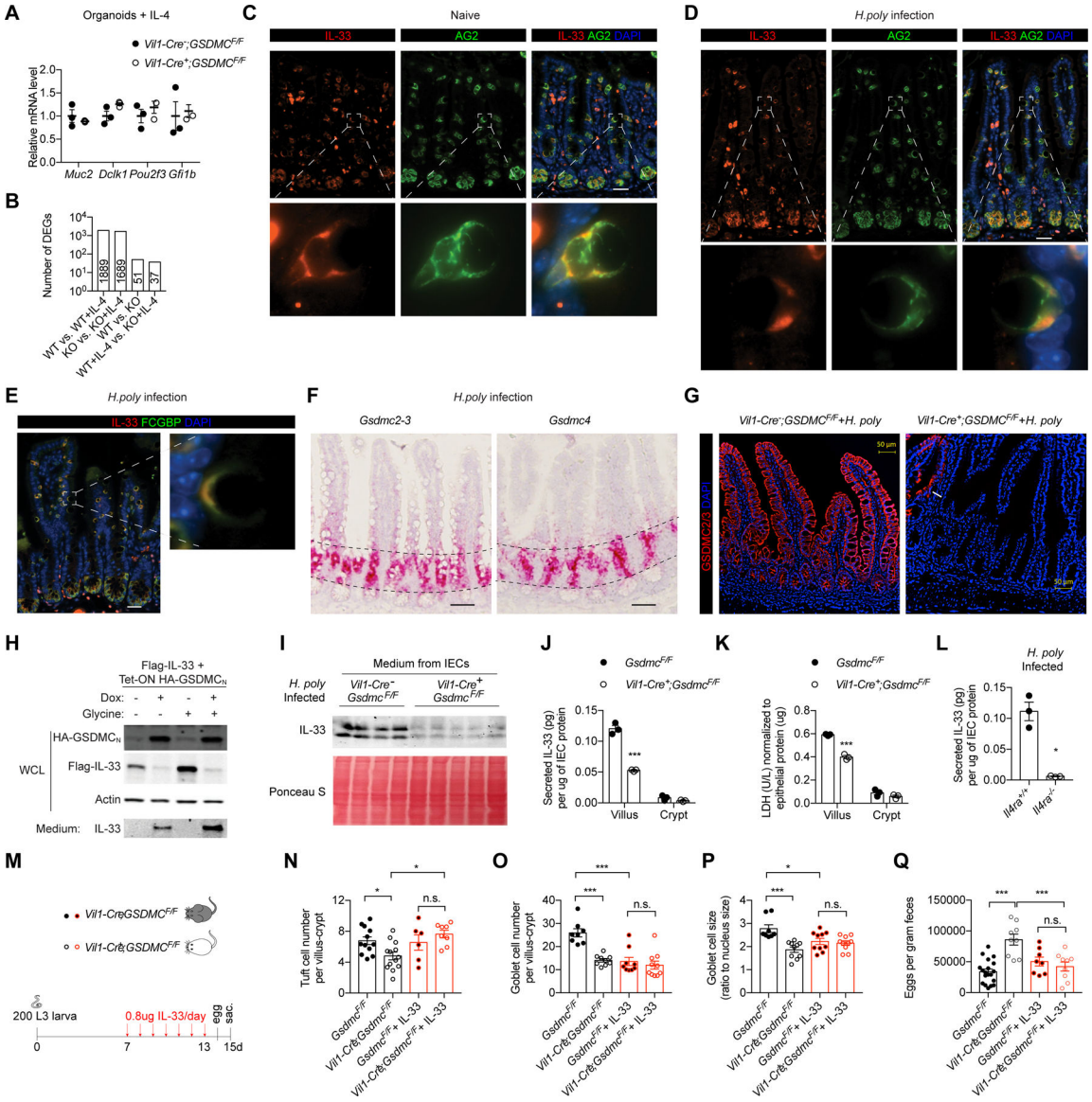

Figure 6. GSDMC$_N$ in goblet cells mediates IL-33 secretion.

(**A**) Expression of tuft cell marker genes in organoids treated with IL-4 (n = 3).

(**B**) Numbers of differentially expression genes among wildtype and IEC$^{\Delta Gsdmc}$ organoids that were treated with or without IL-4 for 2 days.

(**C-E**) Co-staining of IL-33 with goblet cell markers AG2 (C, D) and FCGBP (E) in naïve (C) and *H. polygyrus* infected (D, E) SI.

(**F**) In situ hybridization of *Gsdmc2–3* and *Gsdmc4* mRNA in the SI from *H. polygyrus* infected mice. Dotted lines outline the transient amplifying zone.

(**G**) GSDMC immunofluorescent in the SI from infected mice. White arrow indicates GSDMC-sufficient cells due to the mosaic expression of *Vil1-Cre*. This rare area was deliberately selected to show the specificity of GSDMC antibody.

(**H**) IL-33 and Tet-ON $GSDMC_N$ plasmids were co-transfected into 293 cells, treated with/without doxycycline (Dox) and glycine for 5 h. Whole cell lysate (WCL) and medium were subjected to Immunoblotting.

(**I-K**) Freshly isolated villus (EDTA isolation) and crypt (D-sorbitol/sucrose isolation) IECs from infected mice were cultured for 5 hours, then medium was collected and concentrated for IL-33 Immunoblotting (I, n = 4–5), IL-33 ELISA (J, n = 3), and LDH quantification (K, not concentrated, n = 3).

(**L**) IL-33 secretion from freshly isolated IECs from infected *Il4ra*$^{+/+}$ and *Il4ra*$^{-/-}$ mice was quantified by ELISA (n = 3).

(**M-N**) IEC$^{\Delta Gsdmc}$ mice were infected with *H. polygyrus*, followed with IL-33 treatment for 7 days (M). Tuft cell number (N), goblet cell number (O), goblet cell size (P) and fecal egg output (Q) were shown.

Data are represented as mean ± SEM. * $P < 0.05$, ** $P < 0.01$, *** $P < 0.001$ by one-way ANOVA (M-Q), two-way ANOVA (J, K), or two-tailed unpaired Student's t-test (L). Scale bar = 50 μm. Please also see Figure S6.

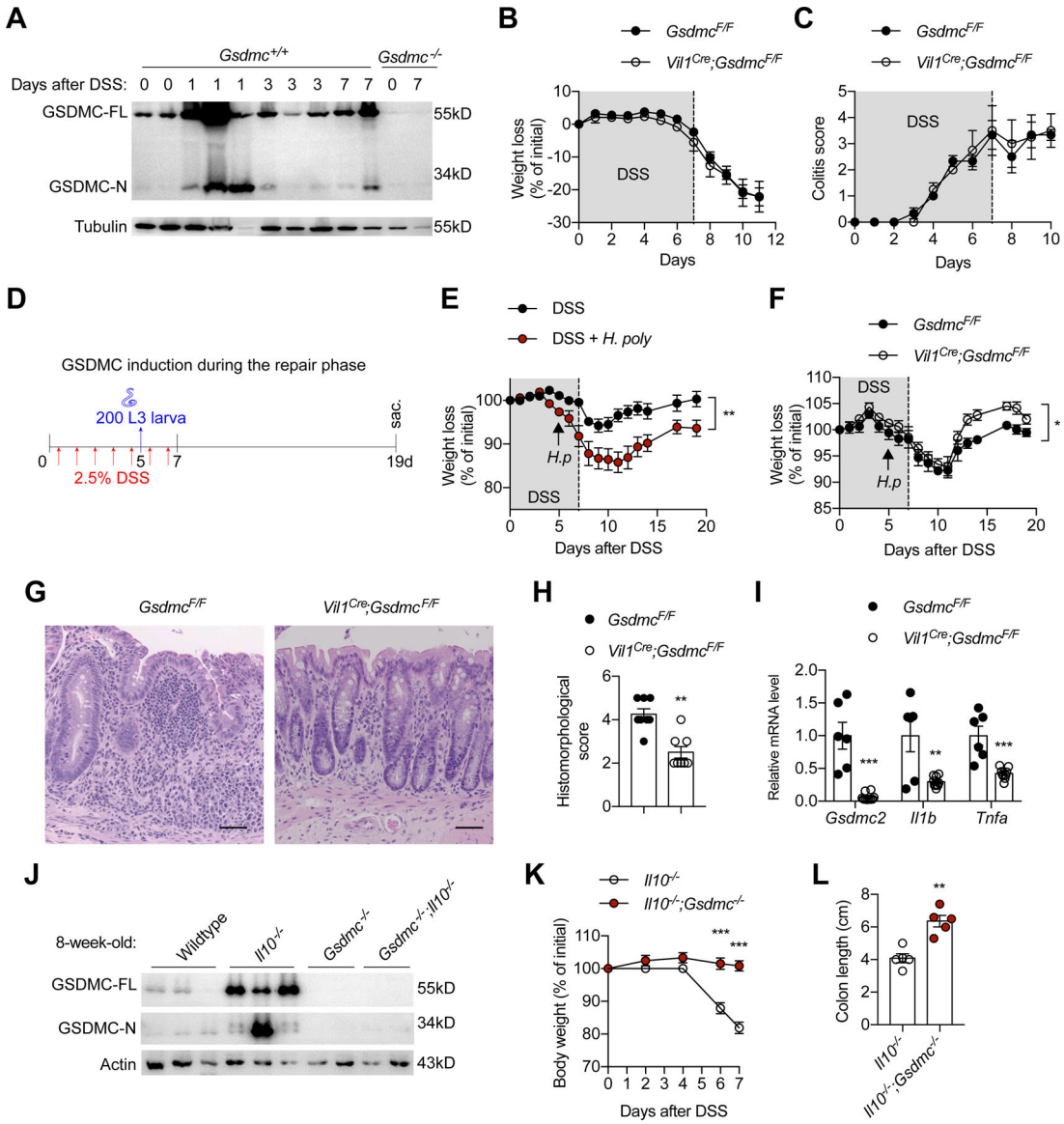

Figure 7. GSDMC drives intestinal type 2 inflammation.

(**A**) Expression of GSDMC protein in the colon during the course of acute DSS colitis.

(**B, C**) Uninfected wildtype (n = 6) and IEC$^{\Delta Gsdmc}$ (n = 4) mice were induced for colitis. Percentage of body weight loss (B) and colitis scores (C) were determined.

(**D**) Timeline for GSDMC induction by *H. polygyrus* infection during the repair phase of DSS colitis.

(**E**) Percentage of body weight loss in C57BL/6 mice that were induced for colitis only (n = 6) or combined with *H. polygyrus* infection on day 5 (n = 7).

(**F-I**) Wildtype and IEC$^{\Delta Gsdmc}$ mice (n = 4) were treated with DSS and then infected with *H. polygyrus* (D). (F) Percentage of body weight loss. (G) Intestinal architecture and immune cell infiltration. Scale bar = 50 μm. (H) Histomorphological score of colitis at the distal colon. 2 areas from each mouse were scored. (I) Expression of intestinal *Gsdmc2–3*, *Il1b*, and *Tnfa* genes.

(**J**) Expression of GSDMC in 8-week old wildtype, *Il10*$^{-/-}$, *Gsdmc*$^{-/-}$, and *Gsdmc*$^{-/-}$;*Il10*$^{-/-}$ mice.

(**K**-**L**) 8-week-old *Il10*$^{-/-}$ (n = 5) and *Gsdmc*$^{-/-}$;*Il10*$^{-/-}$ (n = 5) mice were subjected to acute DSS. Percentage of body weight loss (K) and colon length (L) were measured.

Data are represented as mean ± SEM. * P < 0.05, ** P < 0.01, *** P < 0.001 by two-way ANOVA (E, F, and K) or two-tailed unpaired Student's t-test. Please also see Figure S7.

KEY RESOURCES TABLE

REAGENT or RESOURCE	SOURCE	IDENTIFIER
Antibodies		
Anti-O-GlcNAc antibody	Abcam	Cat# ab2739; RRID: AB_303264
Anti-DCLK1 antibody	Cell Signaling Technology	Cat# 62257S; RRID: AB_2799622
Anti-STAT6 antibody	Cell Signaling Technology	Cat# 5397; RRID: AB_ 11220421
Anti-STAT6 (phospho Y641) antibody (IHC)	Abcam	Cat# ab263947; Lot No: GR3361633
Anti-Phospho-STAT6 (Tyr641) antibody (WB)	Cell Signaling Technology	Cat# 9361; RRID: AB_ 331595
Anti-HA tag antibody	Cell Signaling Technology	Cat# 3724S; RRID: AB_1549585
Anti-OGT antibody	Cell Signaling Technology	Cat# 24083; RRID: AB_2716710
Anti-β-Actin antibody	Millipore Sigma	Cat# A5441; RRID: AB_476744
Anti-Flag M2 antibody	Millipore Sigma	Cat# F3165; RRID: AB_259529
Anti-Tubulin antibody	Santa Cruz	Cat# SC-8035; RRID: AB_628408
Anti-GSDMC2 antibody (WB)	Abclonal	Cat# A12002; RRID: AB_2769695
Anti-GSDMC3 antibody (WB)	Abclonal	Cat# A16741;RRID: AB_2769696
Anti-GSDMC2/3 antibody (IHC)	Abcam	Cat# ab229896; Lot No: GR3317481
Ultra-LEAF™ Purified anti-mouse IL-4 Antibody	Biolegend	Cat# 504122; RRID: AB_11150601
Anti-Anterior Gradient 2 antibody	Abcam	Cat# ab209224; RRID: N/A
Anti-FCGBP antibody	Millipore Sigma	Cat# HPA003517 ; RRID: AB_1078838
Anti-lysozyme antibody	CusAb	Cat# CSBPA02769A0Rb; RRID: N/A
Anti-IL-33 Biotinylated antibody	R&D Systems	Cat# BAF3626; RRID: AB_2124388
IRDye® 800CW Goat anti-Rat IgG Secondary Antibody	Li-Cor	Cat#925-32219; RRID: AB_2721932
IRDye® 680RD Goat anti-Mouse IgG Secondary Antibody	Li-Cor	Cat# 926-68070; RRID: AB_10956588
Alexa Fluor 594 Donkey anti-Mouse Secondary Antibody	Invitrogen	R37115; RRID: AB_2556543
Alexa Fluor 488 Donkey anti-Rabbit Secondary Antibody	Invitrogen	Cat# R37118; RRID: AB_2556546
Chemicals, Peptides, and Recombinant Proteins		
Anti-FLAG® M2 Affinity Gel	Millipore Sigma	Cat# A2220
TRIzol reagent	Invitrogen	Cat# 15596018
iTaq Universal SYBR Green Supermix	Bio-Rad	Cat# 172-5124
RIPA buffer	Millipore Sigma	Cat# 20-188
(Z)-4-Hydroxytamoxifen	Millipore Sigma	Cat# H7904-5MG
Matrigel	Corning	Cat# 354230
Advanced DMEM/F12	Thermo Scientific	Cat# 12634-010
EGF	Peprotech	Cat# AF-100-15
Noggin	Peprotech	Cat# 250-38-100ug
R-spondin 1 conditioned medium	In-house production	N/A
Y-27632	Millipore Sigma	Cat# Y0503
HEPES	Thermo Scientific	Cat # 15630-56
Glutamax	Thermo Scientific	Cat # 35050-038

REAGENT or RESOURCE	SOURCE	IDENTIFIER
Penicillin/Streptomycin	Thermo Scientific	Cat # 15140-122
B-27 supplement (50X)	Gibco	Cat # 17504-044
N2 supplement (100 X)	Gibco	Cat # 17502-048
TrypLE Express Enzyme	Life technologies	Cat #12604013
Polybrene transfection reagent	Millipore Sigma	Cat # TR-1003-G
Nicotinamide	Millipore Sigma	Cat# N0636
CHIR 99021	Axon	Cat# 1386
PBS	Corning	Cat # 21040CV
Vectashield Mounting Medium with DAPI	Vector Laboratories	Cat # H-1500
Alcian-Blue stain kit	Vector	Cat# H-3501
Recombinant Human IL-13	Peprotech	Cat# 200-13
Recombinant Murine IL-4	Peprotech	Cat# AF-214-14
Recombinant Human IL-4	Peprotech	Cat# 200-04
Thiamet-G	CarboSynth	Cat# MD088556
Streptavidin Protein, DyLight 550	Invitrogen	Cat# 84542
ST045849	TimTec	Cat# ST045859
OSMI-1	Millipore Sigma	Cat# SML1621
Endogenous Biotin-Blocking Kit	Invitrogen	Cat# E21390
Lipofectamine™ 2000 Transfection Reagent	Invitrogen	Cat# 11668019
FuGENE® HD Transfection Reagent	Promega	Cat# E2311
Critical Commercial Assays		
Dual-Luciferase Reporter Assay System	Promega	Cat# E1910
BaseScope™ Detection reagent Kit v2-RED	Advanced Cell Diagnostics	Cat# 323900
Mouse IL-33 ELISA kit	Abcam	Cat# ab213475
LDH-Glo Cytotoxicity Assay kit	Promega	Cat# J2380
Experimental Models: Cell Lines		
Human: HEK 293	ATCC	HB-8065
Human: Caco-2	ATCC; share by Dr. Daniel A. Vallera	HTB-37
R-spondin stable cell line	from Dr. Noah Shroyer	N/A
Experimental Models: Organisms/Strains		
Mouse: *Ogt*-floxed	Jackson Laboratory	Cat# 004860
Mouse: *Villin-Cre*	Jackson Laboratory	Cat# 004586
Mouse: *Vil-Ogt* KO	This paper	N/A
Mouse: *Dclk1-CreER*	from Dr. Timothy C. Wang	N/A
Mouse: *Dclk1-Ogt* KO	This paper	N/A
Mouse: *Gsdmc*-floxed and *Gsdmc*-KO	This paper	N/A
Mouse: *Vil-Gsdmc* KO	This paper	N/A
Mouse: *Il-10* KO	Jackson Laboratory	Cat# 002251
Mouse: *Gsdmc/Il-10* DKO	This paper	N/A

REAGENT or RESOURCE	SOURCE	IDENTIFIER
Mouse: *Rosa26-LSL-rOGT*	From Dr. Xiaoyong Yang	N/A
Mouse: *Rosa26-LSL-mOGA*	From Dr. Xiaoyong Yang	N/A
Mouse: C57BL/6J	Jackson Laboratory	Cat# 000664
Mouse: *Stat6* KO	Jackson Laboratory	Cat# 005977
H.polygyrus	from Dr. Jakob von Moltke	N/A
N. brasiliensis	from Dr. Jakob von Moltke	N/A
Oligonucleotides		
Supplemental Table 2	This paper	N/A
Recombinant DNA		
Myc-hOGT plasmid	(Chen et al., 2013)	N/A
Myc-hOGT CD plasmid	(Chen et al., 2013)	N/A
Gsdmc2-luc plasmid	This paper	N/A
Pou2f3-luc plasmid	This paper	N/A
Gsdmc-N-HA plasmid	This paper	N/A
mStat6-Myc-DDK plasmid	Origene	Cat# MR227577
mStat6-Myc-DDK S643A/T644A/T645A plasmid	This paper	N/A
mStat6-Myc-DDK S643A/T644A/T645A plasmid	This paper	N/A
mStat6-Myc-DDK S746A/T757A/S778A plasmid	This paper	N/A
mStat6-Myc-DDK S810/825A plasmid	This paper	N/A
mStat6-Myc-DDK 746-825A plasmid	This paper	N/A
mStat6-Myc-DDK 643-825A plasmid	This paper	N/A
mStat6-Myc-DDK S810/825A plasmid	This paper	N/A
mIL-33 plasmid	Origene	Cat# MR203528
psPAX2	Addgene	Cat# 12260
pMD2.G	Addgene	Cat# 12259
p2xStat6-Luc2P plasmid	Addgene	Cat# 35486
Renilla-luciferase	(Wang et al., 2018)	N/A
Software and Algorithms		
Prism 7	Graphpad	N/A
FIJI (ImageJ2.3.0)	https://imagej.net/Fiji	N/A
Photoshop v11.0	Adobe	N/A
Excel 16.16.27	Microsoft	N/A
Other		